Title
Distributions of trace gases and aerosols during the dry biomass burning season in southern Africa

Journal
Journal of Geophysical Research: Atmospheres, 108(17)

ISSN
0148-0227

Authors
Sinha, P
Hobbs, PV
Yokelson, RJ
et al.

Publication Date
2003-09-16

DOI
10.1029/2003jd003691

Distributions of trace gases and aerosols during the dry biomass burning season in southern Africa

Parikhit Sinha,[1] Peter V. Hobbs,[1] Robert J. Yokelson,[2] Donald R. Blake,[3] Song Gao,[4,5] and Thomas W. Kirchstetter[6]

Received 15 April 2003; revised 8 July 2003; accepted 15 July 2003; published 4 September 2003.

[1] Vertical profiles in the lower troposphere of temperature, relative humidity, sulfur dioxide (SO_2), ozone (O_3), condensation nuclei (CN), and carbon monoxide (CO), and horizontal distributions of twenty gaseous and particulate species, are presented for five regions of southern Africa during the dry biomass burning season of 2000. The regions are the semiarid savannas of northeast South Africa and northern Botswana, the savanna-forest mosaic of coastal Mozambique, the humid savanna of southern Zambia, and the desert of western Namibia. The highest average concentrations of carbon dioxide (CO_2), CO, methane (CH_4), O_3, black particulate carbon, and total particulate carbon were in the Botswana and Zambia sectors (388 and 392 ppmv, 369 and 453 ppbv, 1753 and 1758 ppbv, 79 and 88 ppbv, 2.6 and 5.5 $\mu g\ m^{-3}$, and 13.2 and 14.3 $\mu g\ m^{-3}$). This was due to intense biomass burning in Zambia and surrounding regions. The South Africa sector had the highest average concentrations of SO_2, sulfate particles, and CN (5.1 ppbv, 8.3 $\mu g\ m^{-3}$, and 6400 cm^{-3}, respectively), which derived from biomass burning and electric generation plants and mining operations within this sector. Air quality in the Mozambique sector was similar to the neighboring South Africa sector. Over the arid Namibia sector there were polluted layers aloft, in which average SO_2, O_3, and CO mixing ratios (1.2 ppbv, 76 ppbv, and 310 ppbv, respectively) were similar to those measured over the other more polluted sectors. This was due to transport of biomass smoke from regions of widespread savanna burning in southern Angola. Average concentrations over all sectors of CO_2 (386 ± 8 ppmv), CO (261 ± 81 ppbv), SO_2 (2.5 ± 1.6 ppbv), O_3 (64 ± 13 ppbv), black particulate carbon (2.3 ± 1.9 $\mu g\ m^{-3}$), organic particulate carbon (6.2 ± 5.2 $\mu g\ m^{-3}$), total particle mass (26.0 ± 4.7 $\mu g\ m^{-3}$), and potassium particles (0.4 ± 0.1 $\mu g\ m^{-3}$) were comparable to those in polluted, urban air. Since the majority of the measurements in this study were obtained in locations well removed from industrial sources of pollution, the high average concentrations of pollutants reflect the effects of widespread biomass burning. On occasions, relatively thin (~0.5 km) layers of remarkably clean air were located at ~3 km above mean sea level, sandwiched between heavily polluted air. The data presented here can be used for inputs to and validation of regional and global atmospheric chemical models. *INDEX TERMS:* 0305 Atmospheric Composition and Structure: Aerosols and particles (0345, 4801); 0345 Atmospheric Composition and Structure: Pollution—urban and regional (0305); 3374 Meteorology and Atmospheric Dynamics: Tropical meteorology; *KEYWORDS:* biomass burning, gases, particles

Citation: Sinha, P., P. V. Hobbs, R. J. Yokelson, D. R. Blake, S. Gao, and T. W. Kirchstetter, Distributions of trace gases and aerosols during the dry biomass burning season in southern Africa, *J. Geophys. Res.*, *108*(D17), 4536, doi:10.1029/2003JD003691, 2003.

[1]Department of Atmospheric Sciences, University of Washington, Seattle, Washington, USA.
[2]Department of Chemistry, University of Montana, Missoula, Montana, USA.
[3]Department of Chemistry, University of California, Irvine, California, USA.
[4]Department of Chemistry, University of Washington, Seattle, Washington, USA.
[5]Now at Department of Environmental Science and Engineering, California Institute of Technology, Pasadena, California, USA
[6]Lawrence Berkeley National Laboratory, Berkeley, California, USA.

0148-0227/03/2003JD003691

1. Introduction

[2] Savanna fires in Africa account for about two-thirds of the savanna burned worldwide [*Hao and Liu*, 1994]. Emissions from these fires include carbon dioxide (CO_2), carbon monoxide (CO), nitrogen oxides (NO_x), sulfur dioxide (SO_2), hydrocarbons, halocarbons, oxygenated organic compounds, and particles [*Crutzen and Andreae*, 1990; *Blake et al.*, 1996; *Yokelson et al.*, 1996, 2003; *Andreae and Merlet*, 2001; *Sinha et al.*, 2003a]. In southern Africa most savanna fires occur during the dry season (April–October). In this season the meteorology of southern Africa is characterized by stable air masses, southeasterly trade winds, and subtropical

high pressure over South Africa [*McGregor and Nieuwolt*, 1998]. Also, persistent stable layers, located at ~700 and ~500 hPa restrict vertical mixing of smoke and other pollutants, which results in thick haze layers [*Cosijn and Tyson*, 1996; *Hobbs*, 2002, 2003]. Long-range transport of the pollutants produces elevated concentrations of O_3 over the southern Atlantic Ocean [*Fishman et al.*, 1991, 1996; *Thompson et al.*, 1996]. Pollutants are also transported from southern Africa over the Indian Ocean [*de Laat*, 2002]. During transport, trace gases and particles can be transformed by photochemistry, gas-to-particle conversion, heterogeneous reactions, and particle coagulation [*Liousse et al.*, 1995; *Hobbs et al.*, 1996, 2003; *Goode et al.*, 2000; *Yokelson et al.*, 2003; *Gao et al.*, 2003].

[3] In August and September 2000, the Cloud and Aerosol Research Group (CARG), University of Washington (UW), with its Convair-580 research aircraft, participated in the Southern African Regional Science Initiative 2000 (SAFARI 2000) field project. A previous series of papers has detailed some of the measurements obtained aboard this aircraft in SAFARI 2000. *Sinha et al.* [2003a], *Yokelson et al.* [2003], *Gao et al.* [2003], *Kirchstetter et al.* [2003], *Eatough et al.* [2003], *Pósfai et al.* [2003], and *Li et al.* [2003] described the nature and quantities of gases and particles initially emitted by savanna fires, and *Hobbs et al.* [2003] described the transformations of the initial emissions over short distances. After an hour or two of aging, the smoke is usually visually indistinguishable from the ambient regional haze. The regional haze also ages photochemically, and it is sometimes present in distinct layers that have been transported from different source regions. *Magi et al.* [2003] and *Schmid et al.* [2003] presented regional profiles of light scattering, absorption, and extinction, and *Pilewskie et al.* [2003] calculated solar spectral radiative forcing by aerosols.

[4] In this paper we summarize a large body of observations on ambient regional hazes in southern Africa obtained aboard the UW Convair-580 in SAFARI 2000. Specifically, we present vertical and horizontal distributions of temperature, relative humidity, several important trace gases and particles measured on thirty research flights. Figure 1 shows a photograph of an ambient regional haze layer in the vicinity of Maun, Botswana taken aboard the Convair-580 on September 2, 2000.

2. Sampling Techniques and Instrumentation

[5] A complete list of the instruments aboard the Convair-580 in SAFARI 2000 is given in a technical appendix by P.V. Hobbs in *Sinha et al.* [2003a]. Only the instruments and techniques that provided the measurements presented in this paper are described here.

[6] Continuous measurements of SO_2 were made using a Teco model 43S pulsed-fluorescence analyzer (precision of 7%, detection limit of 0.1 ppbv). Calibration of this instrument, both in flight and on the ground, was carried out prior to, during, and following the field project with a commercial standard mixture (Scott-Marrin) of 180 ± 9 ppbv SO_2 in ultrapure air. The instrument was zeroed using ultrapure air (SO_2 <1 ppbv). Continuous measurements of O_3 were obtained with a Teco model 49C UV photometric analyzer (precision of 2%, detection limit of 3 ppbv). Calibration of this instrument was carried out prior to and following the field project using a Columbia Scientific Instruments Photocal 3000 Version 080 ozonator. The total concentration of particles (CN) in the size range ~0.003–3 μm diameter was measured continuously with a TSI 3025A ultrafine condensation particle counter (precision of 10%).

[7] Evacuated electropolished stainless steel canisters were used to sample ambient air using a stainless steel inlet that passed through the aircraft fuselage. For each canister sample, mixing ratios of selected C_2–C_9 nonmethane hydrocarbons (NMHC) and methyl halides were determined by gas chromatography (GC) with flame ionization detection (FID) and electron capture detection (ECD). The precision of the NMHC and methyl halide measurements was 3%, and the typical NMHC detection limit 3 pptv. Mixing ratios of CO_2 (precision of 3%), CO (precision of 5%), and CH_4 (precision of 0.1%) in the canisters were determined using three separate GC/FID systems. A detailed description of the analytical procedure for the canister samples is given by *Colman et al.* [2001].

[8] An airborne Fourier Transform Infrared Spectrometer (AFTIR), with a separate and specially coated inlet that directed ram air through a Pyrex multipass cell with an exchange time of 4–5 s, was deployed aboard the UW Convair-580. The AFTIR measured CO_2, CO, and CH_4 in ambient air with a precision of ~1%. The AFTIR technique is described by *Yokelson et al.* [2003].

[9] Aerosols with diameter <3 μm were collected on quartz and Teflon filters. The aerosol samples collected on the quartz filters (Pallflex 2500 QAT-UP) were used to determine the concentration of particulate carbon. The quartz filters were baked before use at 800°C for at least 6 hours to remove carbonaceous impurities, and then were analyzed for total carbon (TC) content using the Evolved Gas Analysis (EGA) method described by *Novakov* [1981, 1982] and *Kirchstetter et al.* [2003]. Black carbon (BC) concentrations were measured with an optical transmission technique similar to that described by *Rosen and Novakov* [1983]. This method compares the attenuation of white light through a loaded filter relative to that of a blank filter. The relationship between optical attenuation (ATN) and the BC concentration (μg cm^{-2}) is ATN = σ · BC, where ATN = 100 × ln(I_o/I), I_o and I are the transmitted light intensities through the blank and loaded filters, respectively, and σ the mass attenuation cross-section for BC deposited on the quartz filters (m^2 g^{-1}). As discussed in more detail by *Kirchstetter et al.* [2003], a value of 20 m^2 g^{-1} was used for the mass attenuation cross-section (i.e., calibration factor) based on the work of *Gundel et al.* [1984]. Our use of σ = 20 m^2 g^{-1} is consistent with the calibration factor of a commercial aethalometer that employs the same optical transmission method for measuring BC concentrations [*Bodhaine*, 1995]. Earlier [*Yasa et al.*, 1979] and more recent [*Moosmuller et al.*, 1998] photoacoustic measurements of aerosol light absorption agree well with those of the filter-based light transmission method. While some studies [e.g., *Rosen and Novakov*, 1983, and references therein] assert that the filter-based transmission technique employed in this study is insensitive to light scattering by the collected particles, we note that others have found that such measurements have a measurable response to particle light scattering and thus may overestimate aerosol light absorption (and thus light-absorbing BC). In addition, we

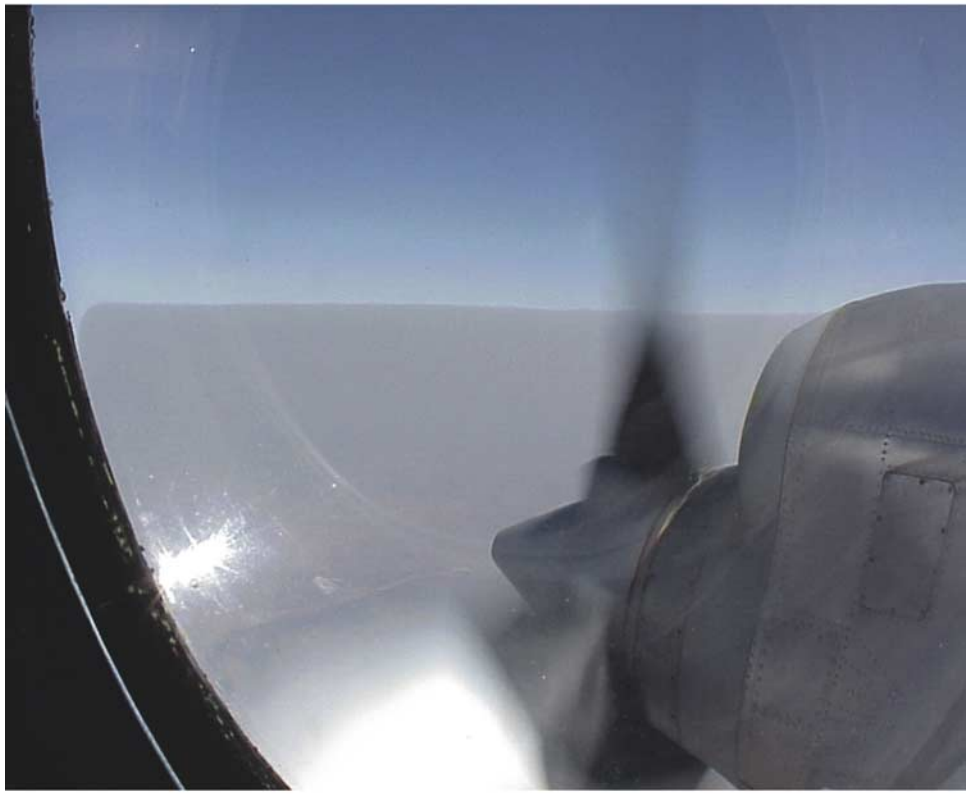

Figure 1. Photograph of ambient regional haze over Botswana (19.97°S, 23.74°E) at 1124 UTC on 2 September 2000. A stable layer at ~4 km msl separates the haze layer from the free troposphere above. (Photo: P. V. Hobbs.)

used a constant value of the mass attenuation cross-section, although others [*Liousse et al.*, 1993; *Petzold et al.*, 1997] have noted that this value may vary with sampling location and aerosol composition.

[10] Particles were also collected on Teflon filters (Gelman Sciences Teflon membrane, 2.0 μm pore size). The Teflon filters were weighed before and after particle sampling in a relative humidity (RH) and temperature (T) controlled chamber (RH = 40%, T = 293 K) to determine the masses of dry particulate matter (PM) collected on the filters. From control and field blank filters, the uncertainty of the total dry PM measured with these filters was estimated to be ±6 μg. After gravimetric analysis, the Teflon filters were extracted in deionized water (HPLC grade) and analyzed by a standard ion chromatography system (Dionex DX 500). This analysis yielded mass concentrations of two inorganic ions (nitrate and sulfate) with a precision of 5%, and seven organic acid ions (acetate, formate, oxalate, malonate, succinate, glutarate, and gluconate) with a precision of 10–20%. An Inductively Coupled Plasma–Atomic Emission Spectrometer (Jarrell Ash 955) was used to measure the mass concentration of the potassium ion to a precision of 4%. Further details on the Teflon filter analyses of aerosol compounds are given by *Gao et al.* [2003].

3. Sampling Locations and Vegetative Types

[11] Vertical profiles were obtained over five sectors of southern Africa that represent four major vegetation classes: the semiarid savannas of northeast South Africa and northern Botswana, the savanna-forest mosaic of coastal Mozambique, the humid savanna of southern Zambia, and the desert of western Namibia (Figure 2a). Most of tropical Africa consists of savanna, which extends from a latitude of ~15°N to ~25°S. Most of the savanna can be broadly classified as humid, extending from ~12°N to ~17°S, while the remainder is semiarid. Savannas are typically found in hot or warm climates where rainfall ranges from 40–130 cm per year and is concentrated in a few months of the year, followed by a long period of drought. Humid savannas typically receive over 60 cm of annual rainfall and have a dry period of less than 6 months per year. Semiarid savannas typically receive less than 60 cm of rainfall per year and have a dry period of greater than 6 months per year [*Huntley*, 1982]. The dense forests of northern Congo, which extend west to the Atlantic Ocean, are an exception to the predominant savanna vegetation of tropical Africa. Also, the deserts of southwest and northern Africa have distinct vegetation. The four vegetation classes in this study account for about one-half of the biomass burned in southern Africa during the dry season of 2000 [*Silva et al.*, 2003].

[12] Sixty-four vertical profiles were obtained during 30 research flights of the Convair-580 in SAFARI 2000. Twenty-five of these profiles were in South Africa, 4 in Mozambique, 7 in Botswana, 14 in Zambia, and 14 in Namibia (Figure 2a and Table 1). The altitudes covered by the profiles ranged from close to ground level up to ~5 km

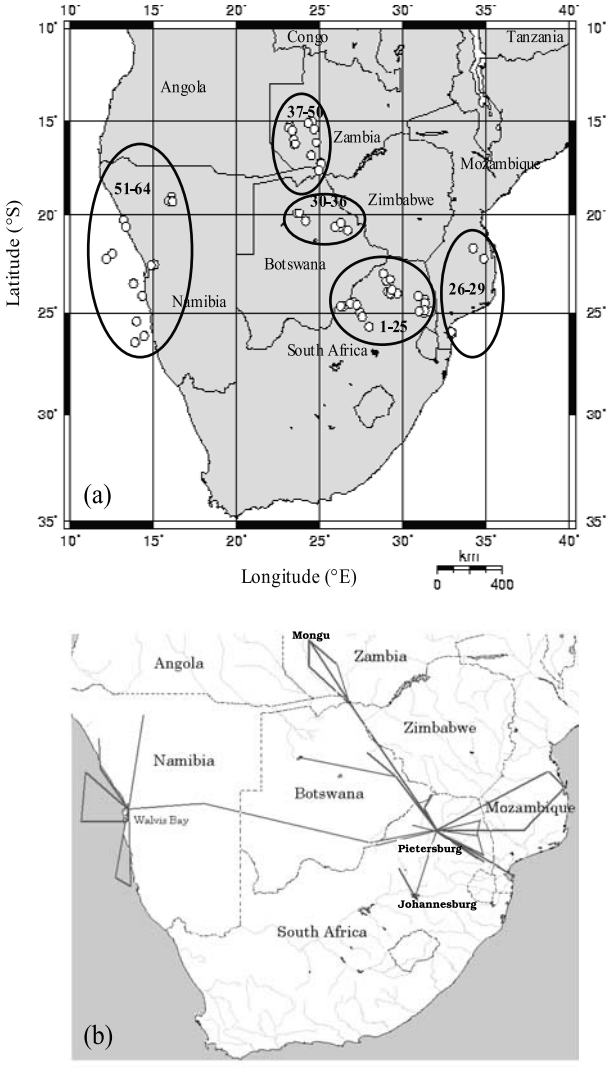

Figure 2. (a) Locations of the vertical profiles obtained aboard the University of Washington's Convair-580 research aircraft in southern Africa during the dry biomass burning season of 2000. Profiles were obtained over five major sectors (within the ovals) in South Africa, Mozambique, Botswana, Zambia, and Namibia. The numbers within each oval are the vertical profile numbers listed in Table 1; the white circles show the locations of the profiles. Note that some of the vertical profiles listed in Table 1 have overlapping locations in this figure. (b) Approximate flight tracks (solid lines) of the UW Convair-580 research aircraft in southern Africa during the dry biomass burning season of 2000. The flying altitude was typically <5 km msl.

above mean sea level (msl). All of the profiles were obtained during daylight hours, and they were all in ambient air, removed from any visible smoke plumes.

[13] The profiles in South Africa were centered around Pietersburg (23.89°S, 29.45°E). The semiarid savanna of this region, locally known as lowveld and highveld depending on altitude, consists of a combination of woodland and bushland savanna. The profiles in Mozambique were near Maputo (25.97°S, 32.60°E) and Beira (19.79°S, 34.92°E). The coastal mosaic of this region consists of a combination of forest and wooded grassland savanna. The profiles in Botswana were east of Maun (19.83°S, 23.50°E) in a region of mopane woodland savanna that also includes the productive wetlands of the Okavanga delta and the halophytic vegetation of the Sua Pan (an expanse of white salt encrusted clay that is the evaporated remains of a lake). The profiles in Zambia were centered around Kaoma (14.78°S, 24.80°E), a region of primarily miombo woodland savanna dominated by the tree species Brachystegia and related genera. The miombo woodland is one of the most prevalent vegetation classes in Africa, covering much of the continent from ~2–17°S. Interspersed through Zambia's miombo woodlands are dambo grasslands; these are affected by seasonal flooding and are covered with a medium-dense, uniform grass mat. The profiles in Namibia were centered around Walvis Bay (22.83°S, 14.50°E), a desert region with a mean annual rainfall of 1 cm. Fog that forms over the cold offshore Benguela current is brought inland by south-westerly winds during the night, contributing another 4–5 cm of mean annual precipitation from fog deposition. Sand dunes, gravel desert, grasses, and succulents characterize this extremely arid region [*White*, 1981, 1983].

[14] The general locations of the horizontal flight tracks of the UW Convair-580 research aircraft in this study are shown in Figure 2b. They cover a wide area of southern Africa from Johannesburg, South Africa in the south, to Mongu, Zambia in the north, and from the Indian Ocean in the east to the South Atlantic Ocean in the west.

4. Climatic Conditions and Fire Frequency

[15] The months from April to October comprise the dry season in southern Africa. For example, Kafue, Zambia (15°S, 26°E) receives 800 cm of rainfall from November to March, while from May to September the rainfall is typically less than 1 cm. Evaporative losses result in a water deficit of >10 cm per month during the dry season in Kafue, leading to water stress for biota, and ultimately a dry and withered savanna that can be readily ignited [*Jury*, 2000]. The rate of biomass burning in southern Africa peaks in the northern part of this region in the early dry season, and a peak in local burning moves south over the course of the dry season arriving in South Africa in September [*Justice et al.*, 1996].

[16] Fire count data for the region is provided by the Along Track Scanning Radiometer (ATSR) aboard the European Remote Sensing-2 satellite. Fire-counts are determined at night-time (~10 pm local time) from ATSR measurements in the 3.7 μm thermal channel. Fire-counts are reported as the number of times the 3.7 μm channel exceeds 308 K [*Arino and Rosaz*, 1999]. The ATSR data show an abundance of fires in southern Africa during the period of this study, August 14–September 16 of 2000 (Figure 3). The South Africa sector contained numerous local fires in August and September, and the western border of the Mozambique sector was lined with fires in August. There were a number of fires within and surrounding the Zambia sector in September. Depending on the prevailing winds, the vertical distribution of pollutants over the Zambia sector could be strongly influenced by aged emissions from fires in Angola, Congo, and Zimbabwe. Since aged smoke is

Table 1. Times, Locations, and Altitudes (msl) for Vertical Profiles of Trace Gases and Aerosols Obtained Aboard the University of Washington's Convair-580 Aircraft in Southern Africa During August and September 2000[a]

Vertical Profile	Date, mm:dd:yy	Time, UTC	Longitude, °E	Latitude, °S	Altitude, km
1	08:14:00	1110–1127	27.95	25.68	1.11–3.64
2	08:14:00	1249–1305	27.40	24.96	1.67–3.45
3	08:14:00	1433–1450	27.53	25.20	0.91–2.74
4	08:14:00	1632–1641	29.26	24.07	1.21–3.29
5	08:17:00	0740–0800	31.23	25.00	0.28–2.99
6	08:17:00	1128–1145	31.28	24.33	0.88–2.99
7	08:18:00	0843–0910	27.01	24.49	0.98–3.33
8	08:18:00	1225–1243	26.42	24.66	1.80–3.98
9	08:18:00	1243–1255	26.82	24.53	2.66–3.97
10	08:18:00	1323–1334	29.16	23.94	1.15–3.34
11	08:20:00	0800–0814	29.06	23.95	1.12–2.86
12	08:20:00	1240–1257	26.23	24.67	1.11–3.12
13	08:20:00	1424–1509	27.20	24.60	1.05–2.86
14	08:20:00	1526–1535	29.21	23.93	1.12–2.89
15	08:22:00	0817–1005	31.65	24.95	0.30–3.60
16	08:22:00	1046–1110	31.30	24.51	0.69–2.49
17	08:22:00	1135–1151	30.90	24.18	0.37–2.50
18	08:22:00	1220–1229	29.63	24.03	1.14–2.49
19	08:23:00	1400–1429	29.21	24.02	1.40–4.53
20	08:29:00	0950–1003	28.80	22.97	1.34–2.65
21	08:29:00	1027–1058	28.99	23.38	1.43–3.74
22	08:29:00	1058–1106	29.31	23.86	1.52–3.74
23	08:29:00	1324–1334	31.28	24.88	0.76–3.32
24	08:29:00	1421–1509	30.95	24.92	0.62–3.06
25	09:06:00	1327–1349	29.21	23.30	1.18–2.72
26	08:24:00	0809–0824	32.95	25.99	0.08–3.90
27	08:24:00	0852–1000	32.88	25.94	0.01–2.53
28	08:31:00	1017–1055	34.84	22.23	0.03–2.78
29	08:31:00	1227–1250	34.20	21.71	0.40–3.72
30	09:02:00	0952–1010	23.62	19.91	0.92–4.29
31	09:02:00	1058–1127	23.74	19.88	2.02–4.27
32	09:02:00	1127–1140	24.13	20.31	2.70–4.30
33	09:03:00	0816–0830	26.65	20.79	2.98–4.44
34	09:03:00	0830–0844	26.21	20.61	1.01–4.40
35	09:03:00	1009–1036	25.90	20.63	0.89–4.44
36	09:03:00	1045–1055	26.25	20.42	2.22–4.41
37	09:01:00	0745–0804	25.03	17.27	1.72–3.00
38	09:01:00	0831–0845	24.52	15.02	2.14–2.99
39	09:01:00	1010–1030	24.63	15.41	1.81–3.62
40	09:01:00	1048–1057	25.06	17.32	1.91–3.67
41	09:05:00	1054–1155	24.76	16.16	1.26–3.97
42	09:05:00	1257–1306	24.28	15.10	1.54–3.11
43	09:05:00	1319–1325	23.43	15.98	1.46–3.03
44	09:05:00	1325–1333	23.45	16.27	1.49–3.48
45	09:05:00	1357–1408	24.94	17.63	1.11–3.41
46	09:06:00	0744–0758	23.51	16.22	1.08–3.61
47	09:06:00	0915–0932	23.16	15.24	1.13–4.54
48	09:06:00	0932–0951	23.11	15.34	1.47–4.55
49	09:06:00	0951–1009	23.32	15.49	1.47–4.75
50	09:06:00	1015–1055	24.47	16.87	1.00–5.05
51	09:10:00	1008–1021	15.04	22.53	0.04–3.58
52	09:11:00	0923–0935	12.52	21.98	0.58–3.62
53	09:11:00	0957–1040	12.15	22.23	0.38–2.88
54	09:11:00	1109–1138	13.78	23.54	0.86–3.50
55	09:13:00	1113–1134	13.20	20.26	0.84–4.89
56	09:13:00	1134–1312	13.33	20.61	0.33–4.91
57	09:14:00	0854–0912	14.42	26.13	1.72–2.96
58	09:14:00	0916–0953	13.86	26.45	0.02–1.92
59	09:14:00	1126–1140	13.96	25.41	0.12–3.59
60	09:14:00	1140–1227	14.32	24.15	0.12–3.58
61	09:16:00	0840–0854	16.07	19.01	1.19–4.24
62	09:16:00	1052–1108	15.90	19.21	1.07–4.59
63	09:16:00	1108–1128	16.14	19.26	1.79–4.52
64	09:16:00	1221–1239	14.84	22.56	0.16–3.07

[a]Profiles 1–25 were over the South Africa sector, profiles 26–29 were over the Mozambique sector, profiles 30–36 were over the Botswana sector, profiles 37–50 were over the Zambia sector, and profiles 51–64 were over the Namibia sector.

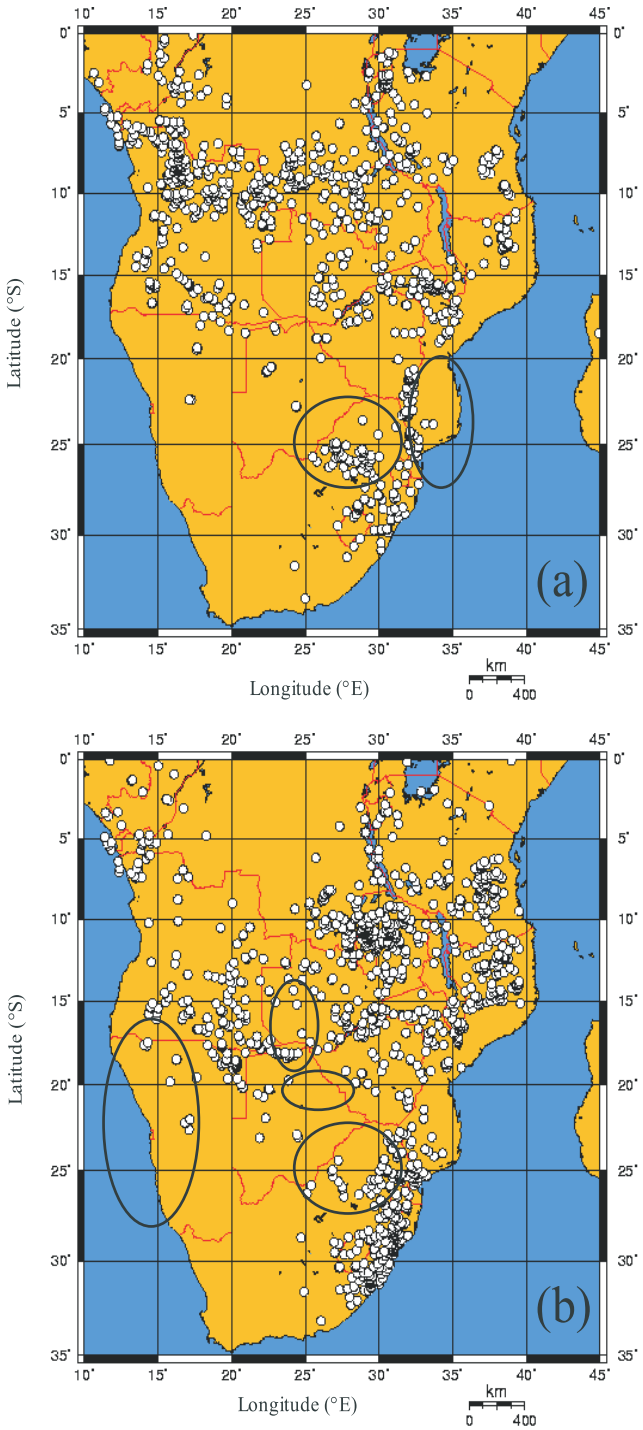

Figure 3. Fire counts from the Along Track Scanning Radiometer (ATSR) aboard the European Remote Sensing-2 Satellite at ~10 pm local time in (a) August and (b) September 2000. Locations of the five sets of vertical profiles of the UW Convair-580 aircraft were within the ovals.

typically enhanced in oxidation products and oxidation by-products such as organic acids and ozone [*Hobbs et al.*, 2003], the lower atmosphere in Zambia contained large concentrations of these pollutants. As with the Zambia sector, there were abundant fires surrounding the landlocked Botswana sector, with possible transport of fire emissions from Angola, Zambia, Zimbabwe, South Africa, and Mozambique. Transport of emissions into Namibia from the fire-prone area of southern Angola affected the vertical distribution of pollutants in this region.

[17] The climatological mean atmospheric circulation in southern Africa in the dry season is depicted in Figure 4a (Realtime Environmental Applications Display System (READY), FNL archive, 2002, available at www.arl.noaa.gov/ready.html). It is characterized by a semipermanent continental gyre with easterly winds in the tropical band (10°–20°S), westerly winds in the temperate band (20°–

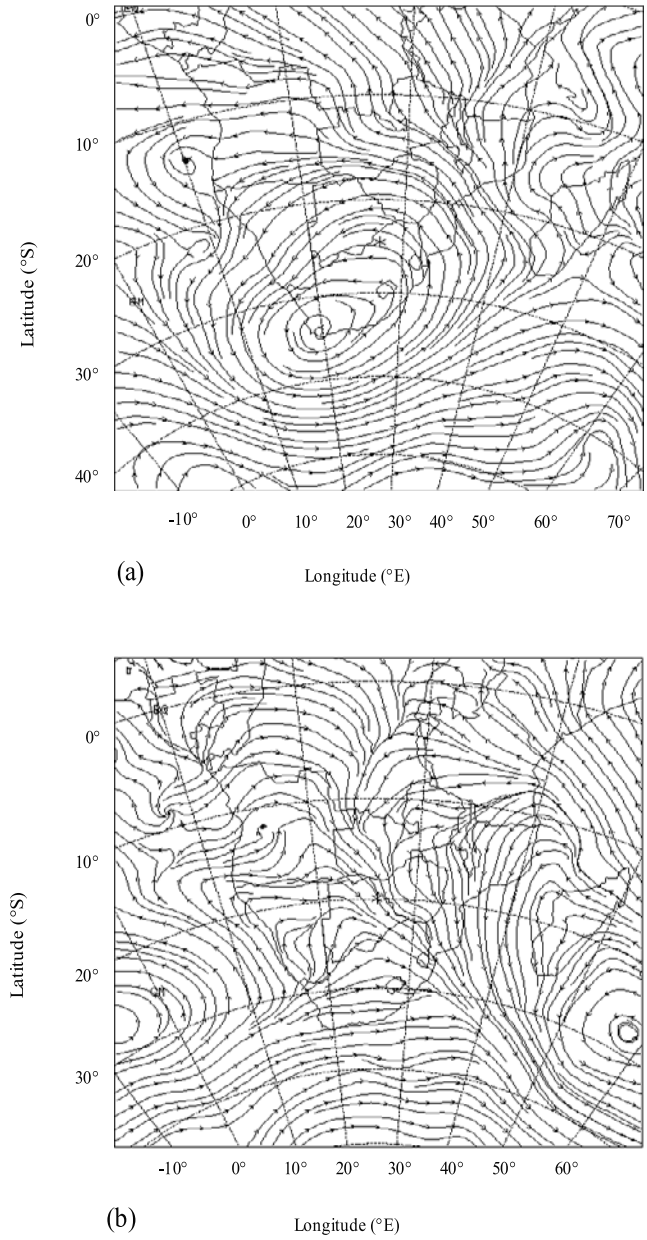

Figure 4. The 850 hPa streamlines for (a) 1200 UTC August 14, 2000, and (b) 1200 UTC September 3, 2000. The streamlines in Figure 4a reflect the climatological mean continental gyre, and Figure 4b shows the passage of a westerly trough (from READY, FNL archive, 2002, available at www.arl.noaa.gov/ready.html).

30°S), and meridional winds over the east and west coasts of Africa around 20°S [*Jury*, 2000]. The transport of smoke from savanna fires under the conditions of the continental gyre are reflected in measurements of the aerosol index from the NASA Total Ozone Mapping Spectrometer (TOMS), which are shown in Figure 5a. Smoke from fires in Angola, Congo, and Zambia are transported westward and accumulate over the southern Atlantic Ocean. This long-range transport of pollutants, termed the ''great African plume'' by *Chatfield et al.* [1998], occurs when biomass burning emissions, which mix into a ~3–4 km deep boundary layer over southern Africa, override cooler air from the rainforests of the central Congo, and then head westward over the south Atlantic Ocean. This plume is a predominant source of pollution in the midtropical southern Atlantic Ocean [*Chatfield et al.*, 1998].

[18] On average, the continental gyre prevails approximately half the time during the dry season and is perturbed by westerly waves with a ~30% frequency [*Jury*, 2000]. For example, a westerly trough in early September 2000 produced the northwesterly flow shown in Figure 4b. This resulted in smoke being transported southeastward from central Africa to the Indian Ocean (Figure 5b). This event, termed the ''river-of-smoke'' by *Annegarn et al.* [2003], resulted in heavy haze and reduced visibility over southern Africa for about ten days in early September 2000.

[19] During August 2000 weather conditions were consistent with the climatological mean conditions summarized above, with the continental gyre prevailing about half the time and perturbations by westerly waves present on approximately 1 out of 3 days. However, conditions were more unstable in September 2000, with frequent penetrations by frontal perturbations and unstable air masses, including the river-of-smoke [*Freiman et al.*, 2002].

[20] Vertical air motions over southern Africa during the dry season are driven by sensible heating of the surface by solar radiation, resulting in vigorous vertical fluxes and an atmospheric mixed layer ~3 km in depth over southern Africa during the daytime [*Jury*, 2000]. Above the mixed layer are persistent capping stable layers at ~700 and ~500 hPa (~3 and ~5.5 km msl, respectively), which are produced by strong subsidence. These stable layers are ~0.5–1 km thick and trap pollutants below their bases by inhibiting vertical mixing. Capping stable layers were observed in southern Africa on nine out of ten days during August and September, 2000 [*Freiman et al.*, 2002].

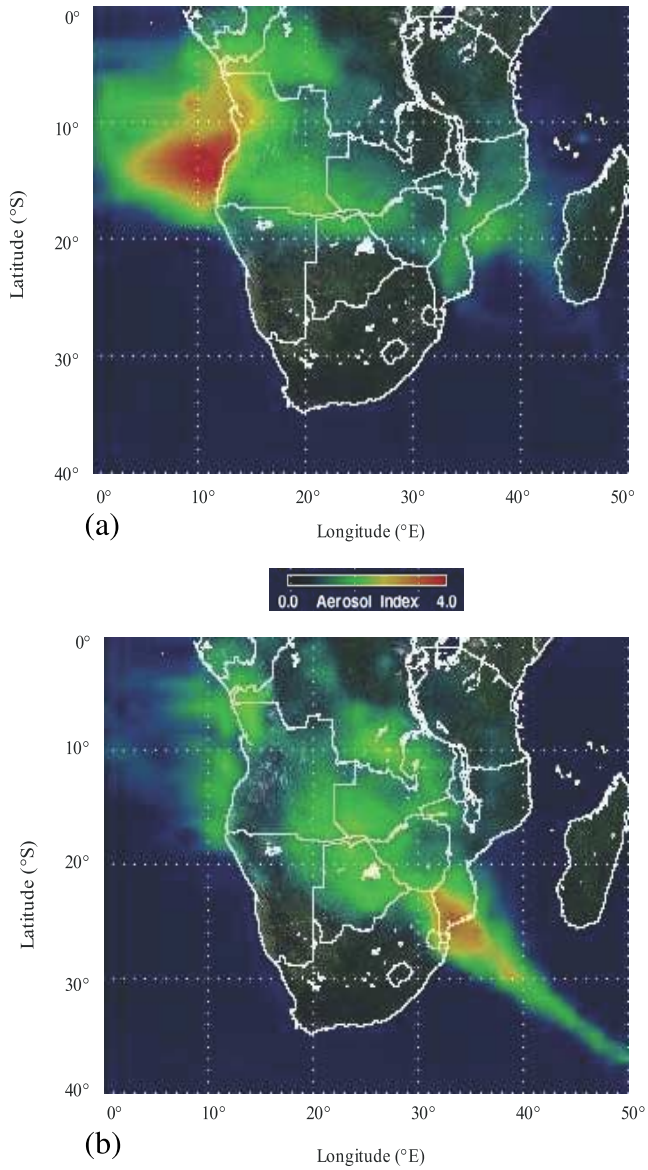

Figure 5. TOMS aerosol index for (a) September 7, 2000, under conditions of the continental gyre shown in Figure 4a, and (b) September 4, 2000, during the passage of the westerly trough shown in Figure 4b [from *Privette et al.*, 2001]. The aerosol index is related to aerosol optical depth; visibility decreases as the aerosol index increases from 0 to 4.

5. Industrial Sources and Domestic Burning

[21] The region of northeast South Africa where the vertical profiles 1–25 (Figure 2a and Table 1) were obtained includes the Kruger National Park and other wildlife preserves, which are characterized by vast tracts of semiarid savanna. It is also a region of intense power production and mining operations, where some 95% of South Africa's electricity is generated primarily by coal-fired power plants [*Energy Information Administration* (*EIA*), 2002]. Several of the largest of these plants are located in the Mpumalanga province of South Africa, which includes Kruger National Park. Some of the vertical profiles presented in this paper were obtained over this region. Many of South Africa's mining operations are also located in northeast South Africa, including 81% of South Africa's coal mines [*EIA*, 2002] and the Palaborwa copper mine, one of the largest copper mines in the world. The heavy machinery required for mining operations are energy intensive and can result in high emissions of pollutants. Airborne measurements obtained in this study in the plume from the Palaborwa mine show an excess of ~15 ppbv of SO_2 above ambient levels. For comparison, an excess of 7–64 ppbv of SO_2 above ambient levels were measured in the smoke plume from a large, vigorous savanna fire in the nearby Timbavati Game Park [*Hobbs et al.*, 2003].

[22] Profiles 26–29 (Figure 2a and Table 1) were obtained over the Indian Ocean coast of Mozambique, a region of coastal forest and savanna. With a primarily

agricultural society, there are few industrial sources of pollution in this sector, leaving biomass burning as the major local source of air pollution.

[23] Profiles 30–36 (Figure 2a and Table 1) were obtained over northern Botswana, a region of woodland savanna, wetlands, and salt pans. Botswana is a primarily agricultural society with a small population (<2 million). Except for diamond mining, there are few industrial sources of pollution in this region.

[24] Profiles 37–50 (Figure 2a and Table 1) were obtained over the upper Zambezi River Valley, a region of humid savanna where industrial emissions are minor. However, the "copper belt" north of the Zambia sector, situated between Zambia and the Democratic Republic of Congo, is a focus of mining and development activities and contains 34% and 10% of global cobalt and copper reserves, respectively (Mbendi, Information for Africa, 2003, available at http://www.mbendi.co.za/index.htm).

[25] Profiles 51–64 (Figure 2a and Table 1) were obtained over the Namib Desert and the adjacent South Atlantic coast of Namibia. The cold, upwelling waters of the Benguela current off the Namibian coast support a diverse marine ecosystem and a strong fishing industry based out of Walvis Bay, Namibia. Ocean-going vessels are among the world's highest polluting combustion sources per quantity of fuel consumed. For example, emission factors of NO_x (as NO) and SO_2 from ships sampled off the coast of Namibia were 21–69 and 3–56 g per kg fuel burned, respectively [*Sinha et al.*, 2003b], compared to only 3.3 ± 0.6 and 0.43 ± 0.30 g per kg fuel burned, respectively, for savanna fires in southern Africa [*Sinha et al.*, 2003a]. Since relatively few savanna fires occur in Namibia, emissions from ships could have an impact on air quality along the Namibian coast.

[26] In addition to emissions from savanna fires and industrial sources, air quality in southern Africa is substantially affected by biofuel use, since the majority of residential energy for heating and cooking comes from the burning of fuel wood and charcoal. Unlike savanna burning, which is seasonal, biofuel use occurs year-round. Therefore, annual emissions of several important trace gases (e.g., CH_4) from biofuel use rival or even exceed those from savanna fires [*Bertschi et al.*, 2003a]. Biofuel use is commonplace throughout southern Africa, accounting for 75% of total energy consumption in the region [*EIA*, 2002]. Of the five sectors in this study, biofuel use is highest in South Africa, Mozambique, and Zambia where ~8–9 Tg of fuel wood are burned annually per country, compared to <1 Tg yr^{-1} per country for Botswana and Namibia [*Yevich and Logan*, 2003].

6. Vertical Profiles

[27] Vertical profiles of temperature, relative humidity (RH), SO_2, O_3, and CN over the South Africa, Mozambique, Botswana, Zambia, and Namibia sectors are summarized in Figures 6–10. In these figures, the numerous measurements obtained in the profiles over each sector (Table 1) are summarized in boxes in which mean, median, and several percentile values are given for various altitudes. In the remainder of this paper, all altitudes will refer to height above msl.

[28] Before discussing the results shown in Figures 6–10, we will describe briefly the importance of SO_2, O_3 and CN, and, for comparison, some typical values of these species in various environments. Sulfur dioxide is the primary anthropogenic sulfur-containing air pollutant. Upon oxidation to sulfate, SO_2 contributes to acidity and light scattering in the atmosphere. The lifetime of SO_2 through oxidation by the hydroxyl radical (OH) is about one week. However, SO_2 in the boundary layer can be removed by dry deposition on a timescale of a day, and even more rapidly by wet deposition. Typical mixing ratios for SO_2 in clean, continental air and in polluted, continental air are ~0.2 and 1.5 ppbv, respectively [*Seinfeld and Pandis*, 1998].

[29] Tropospheric O_3 can damage vegetation and is deleterious to human health. It is an important precursor of OH, the primary oxidant in the troposphere. Ozone is also an important greenhouse gas in the upper troposphere [*Mauzerall et al.*, 1998]. The photochemical lifetime of O_3 is ~10 days and depends on season and latitude. Ozone can also be removed from the troposphere by dry deposition on a timescale of about a month. Typical mixing ratios for O_3 in remote locations range from ~20–40 ppbv; in polluted urban air it can exceed 100 ppbv [*Seinfeld and Pandis*, 1998]. Ozone mixing ratios in smoke from savanna fires are comparable to those in polluted urban air. For example, ~20 km downwind of a 1000 ha savanna fire in the Timbavati Game Park, O_3 mixing ratios in excess of 100 ppbv were measured [*Hobbs et al.*, 2003].

[30] Particles in the troposphere reduce visibility, they play a role in heterogeneous chemistry, they are involved in the formation of cloud droplets, and they affect atmospheric radiation. Particles can be removed by coagulation and dry and wet deposition. Particles smaller than ~0.01 μm in diameter and larger than ~20 μm in diameter have lifetimes less than about a day. However, accumulation-mode particles (0.1–3 μm diameter) may reside in the troposphere for weeks or months [*Hobbs*, 2000]. The concentrations of CN typically range from ~10,000–400,000 cm^{-3} for polluted, continental locations, ~2,000–10,000 cm^{-3} for rural sites over continents, ~50–10,000 cm^{-3} for remote, continental sites, and ~100–400 cm^{-3} for marine locations [*Seinfeld and Pandis*, 1998]. The CN concentrations over the Timbavati fire ranged from ~500,000 cm^{-3} over the fire to ~30,000 cm^{-3} 30 km downwind [*Hobbs et al.*, 2003].

[31] In addition to the vertical profiles of temperature, relative humidity, SO_2, O_3, and CN, we obtained less detailed profiles of CO (from intermittent samples) over South Africa, Mozambique, Botswana, Zambia, and Namibia. The lifetime of CO in the tropics is ~1 month [*Seinfeld and Pandis*, 1998]. In the background troposphere, CO concentrations range from ~50–150 ppbv in remote areas, to ~1000 ppbv in rural-suburban areas, to several ppm in polluted urban areas [*Finlayson-Pitts and Pitts*, 2000]. The mixing ratios of CO in initial smoke from savanna fires are comparable with those in polluted urban air. For example, in the Timbavati plume the CO mixing ratios ranged from ~3.5–5.7 ppmv [*Hobbs et al.*, 2003].

6.1. Temperature and Relative Humidity

[32] Figures 6a, 7a, 8a, 9a, and 10a (6a–10a) summarize the vertical profiles of temperature over the South Africa, Mozambique, Botswana, Zambia, and Namibia sectors, respectively. Over the South Africa sector, the average lapse rate from 0.5–3 km was ~8.5° km^{-1} (Figure 6a),

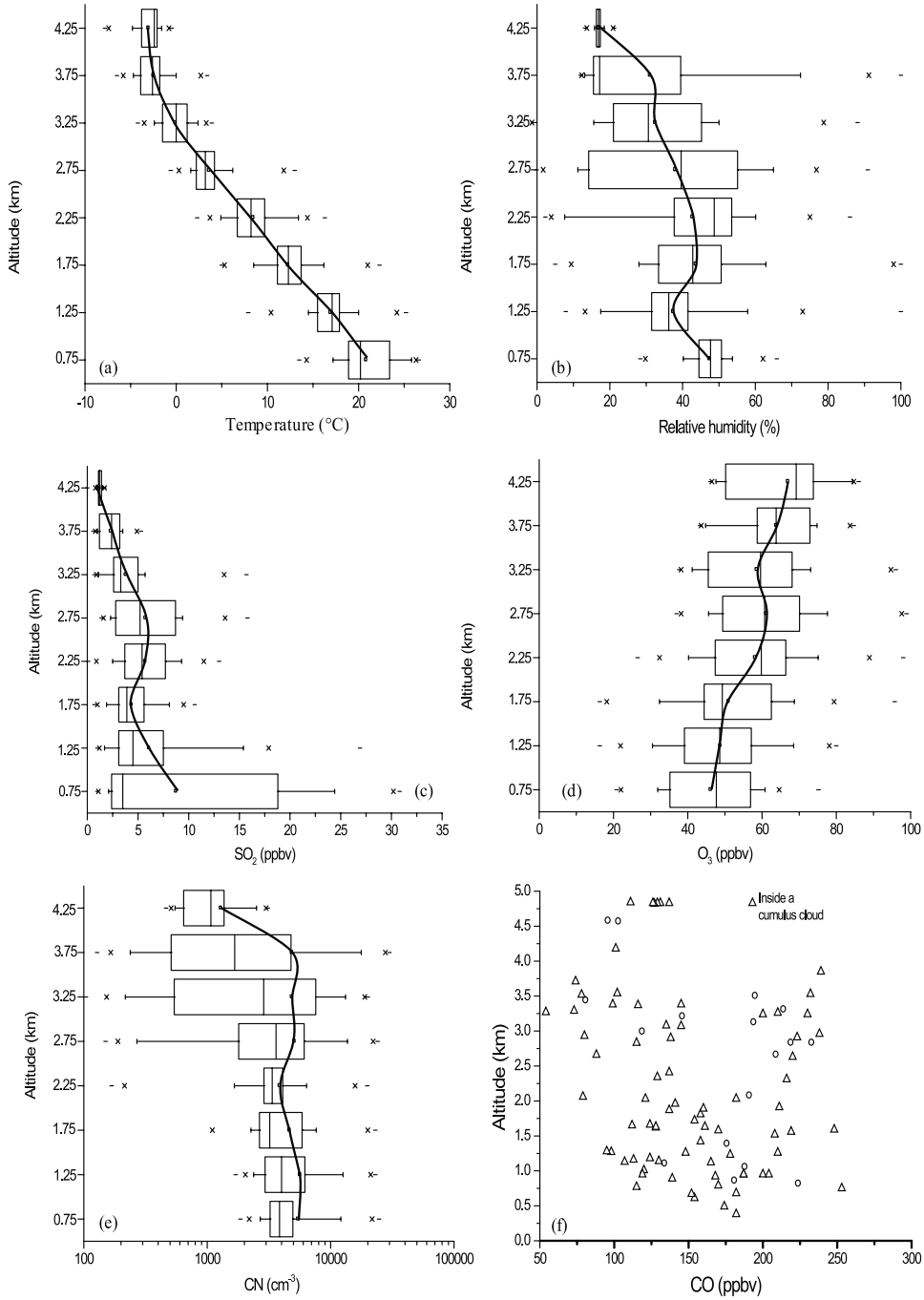

Figure 6. Summary of vertical profiles 1–25 (from Table 1) of (a) temperature, (b) relative humidity, (c) SO_2, (d) O_3, and (e) CN over the South Africa sector for the period August 14 to September 6, 2000. In Figures 6a–6e the square symbol in each box denotes the mean of the data; the vertical line within each box denotes the 50th percentile value; the left and right sides of each box denote the 25th and 75th percentile values, respectively; and, the error bars denote the 5th and 95th percentile values. The two symbols to the left of the 5th percentile error bar denote the 0th and 1st percentile values, and the two symbols to the right of the 95th percentile error bar denote the 99th and 100th percentiles. (f) Intermittent samples of CO over the South Africa sector, with the circles and triangles indicating measurements by GC/C and AFTIR, respectively.

which is intermediate between the dry adiabatic lapse rate of 9.8° km^{-1} and the saturated adiabatic lapse rate of typically 6–7° km^{-1}. Thus, the atmosphere was generally conditionally unstable below 3 km. Above 3.5 km, the average lapse rate over South Africa (~3°C km^{-1}) was less than both the dry and saturated adiabatic lapse rate, resulting in a stable layer below which pollutants were trapped. Hence, during the period of our measurements, temperature

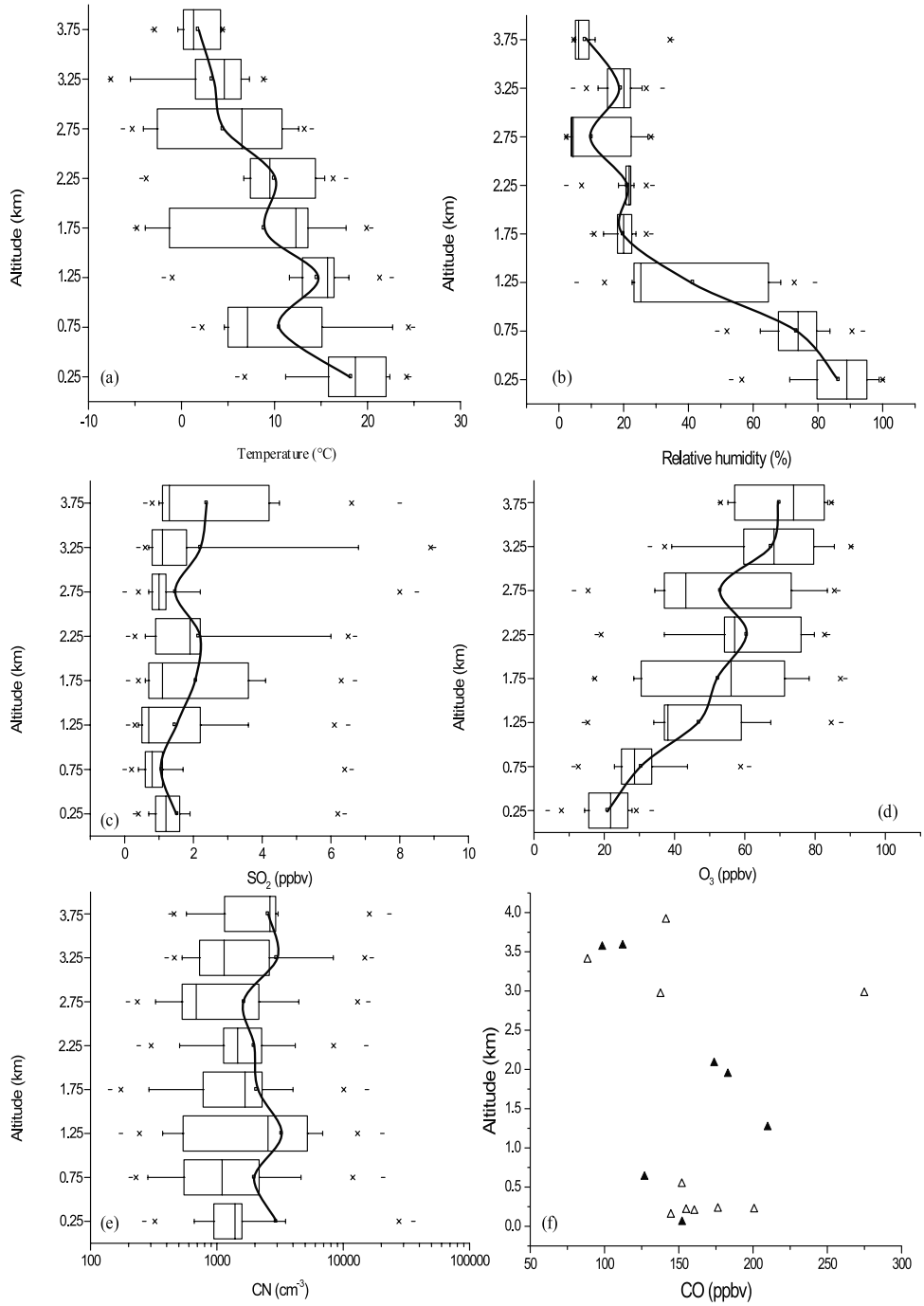

Figure 7. (a)–(e) As for Figure 6, but for vertical profiles 26–29 (from Table 1) over the Mozambique sector for the period of August 24–31, 2000. (f) Intermittent samples of CO over the Mozambique sector obtained by AFTIR, with the open and closed triangles indicating continental and maritime measurements, respectively.

profiles over the South Africa sector were consistent with the climatological average conditions of a mixed layer up to ~3 km, capped by a stable layer.

[33] Over the Mozambique sector, the lapse rate was close to adiabatic near the surface (Figure 7a). Above this neutral layer, temperature inversions were present from ~0.75–1.25 km and ~1.75–2.25 km. Above the second inversion was another neutral layer from ~2.25–2.75 km. Above ~2.75 km, the lapse rate was ~3° km^{-1}, less than both the dry and saturated adiabatic lapse rates, resulting in another stable layer below which pollutants were trapped. This last stable layer is consistent with the climatological average conditions of a stable layer at ~3 km. However, the presence of two inversion layers below the 3 km stable layer resulted in increased stratification of the lower atmosphere over the Mozambique sector.

[34] For the Botswana sector, the average lapse rates from ~1.25–2.25 km and from ~2.75–3.25 km were greater

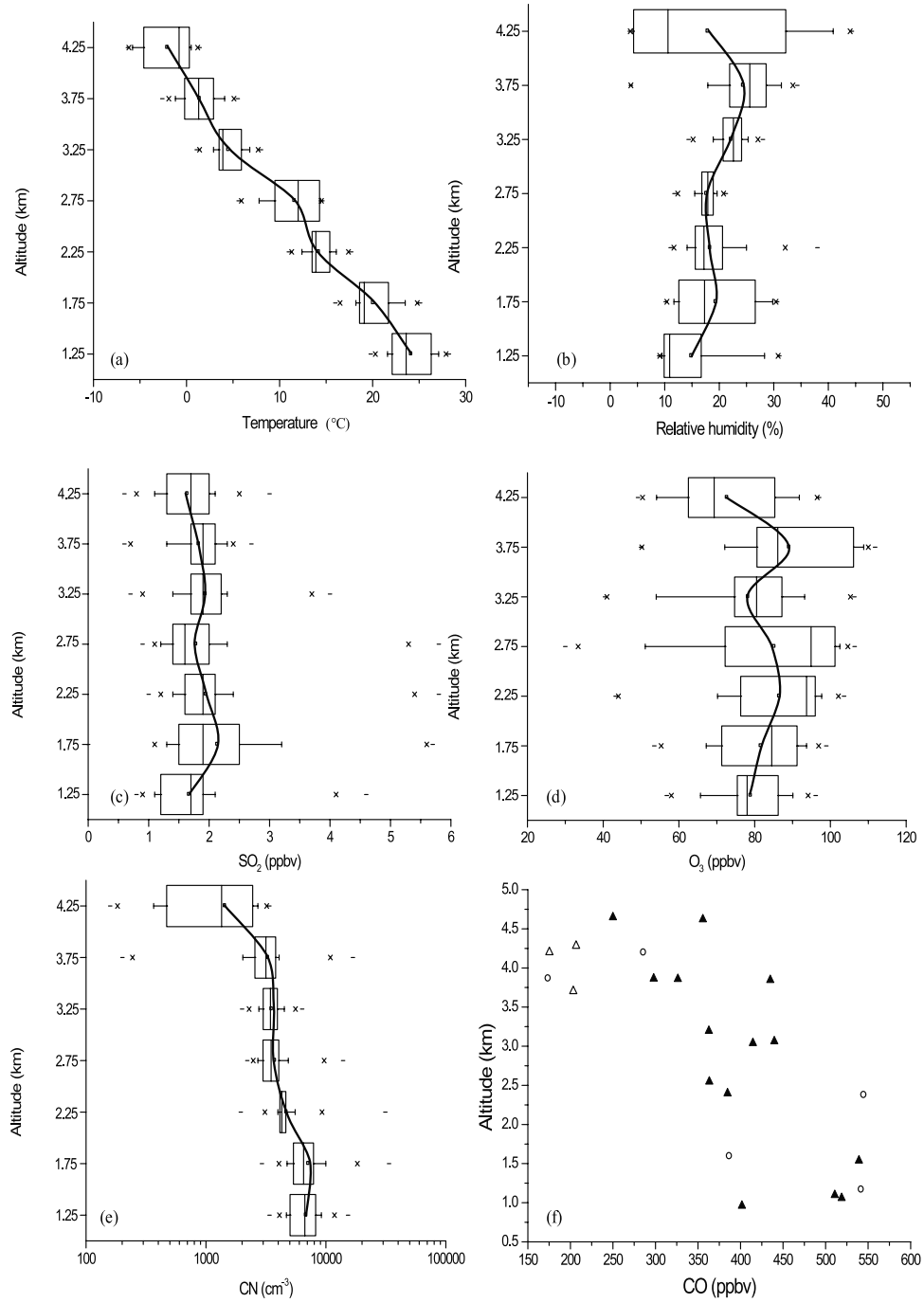

Figure 8. (a)–(e) As for Figure 6, but for vertical profiles 30–36 (from Table 1) over the Botswana sector for the period of September 2–3, 2000. (f) Intermittent samples of CO over the Botswana sector, with the open triangles indicating AFTIR measurements obtained on 1 September 2000, the closed triangles indicating AFTIR measurements obtained on 3 and 6 September 2000, and the circles indicating GC/C measurements obtained on 1–3 September 2000.

than the adiabatic lapse rate, resulting in unstable conditions over these altitudes (Figure 8a). Stable layers occurred from ~2.25–2.75 km and from ~3.25–4.25 km, where the lapse rates were only ~6° km^{-1}. Since ground level in this region is at ~1 km, and the first stable layer occurred around 2.5 km, the surface mixed layer was only ~1.5 km deep.

[35] With the exception of two stable layers from ~2.25–2.75 km and from ~3.75–4.25 km, the lapse rate in the Zambia sector was greater than dry adiabatic, which resulted in an unstable atmosphere (Figure 9a). The observed stable layers at ~2.5 km and ~4 km were somewhat lower in altitude than the climatological stable layers, which are situated at ~3 km and ~5.5 km. However, the 0.5 km thickness of the observed layers is within the range of the climatological average thickness of ~0.5–1 km.

[36] Over the Namibia sector, a persistent coastal stratus cloud deck was present below ~1 km. Above the cloud deck, distinct temperature inversions were present from

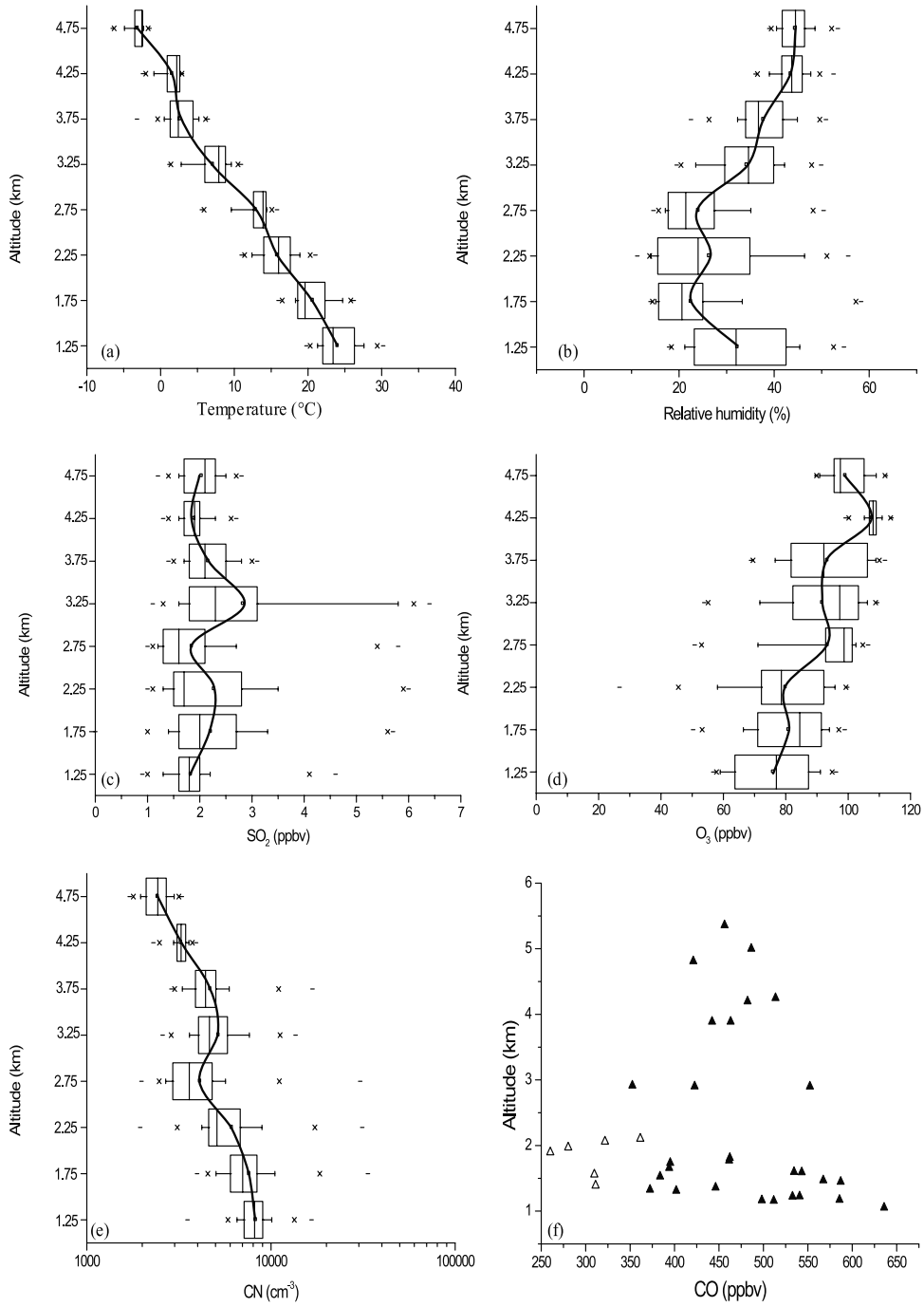

Figure 9. (a)–(e) As for Figure 6, but for vertical profiles 37–50 (from Table 1) over the Zambia sector for the period of September 1–6, 2000. (f) Intermittent samples of CO over the Zambia sector, with the open and closed triangles indicating measurements obtained by AFTIR on 1 September 2000 and 5–6 September 2000, respectively.

~0.75–1.25 km and ~1.75–2.25 km (Figure 10a). Above ~3.5 km, the lapse rate was close to dry adiabatic, resulting in a neutral atmosphere.

[37] Figures 6b–10b summarize the vertical profiles of relative humidity over the South Africa, Mozambique, Botswana, Zambia, and Namibia sectors, respectively. *Magi and Hobbs* [2003] found that over southern Africa during the dry season in 2000 the aerosol total light scattering coefficient increased by a factor of ~1.5–2 when relative humidity increased from 30% to 80%. Relative humidity over the South Africa sector during the period of our study ranged from ~20–60% and generally decreased with increasing altitude. Over the coastal Mozambique sector, RH was high (~60–100%) below 1 km and decreased to <20% above ~1.5 km. There was a local minimum at ~2.75 km, where the median RH was only 4%. Relative humidity over the Botswana sector was low (<30%) and fairly uniform with height. The RH over the Zambia sector

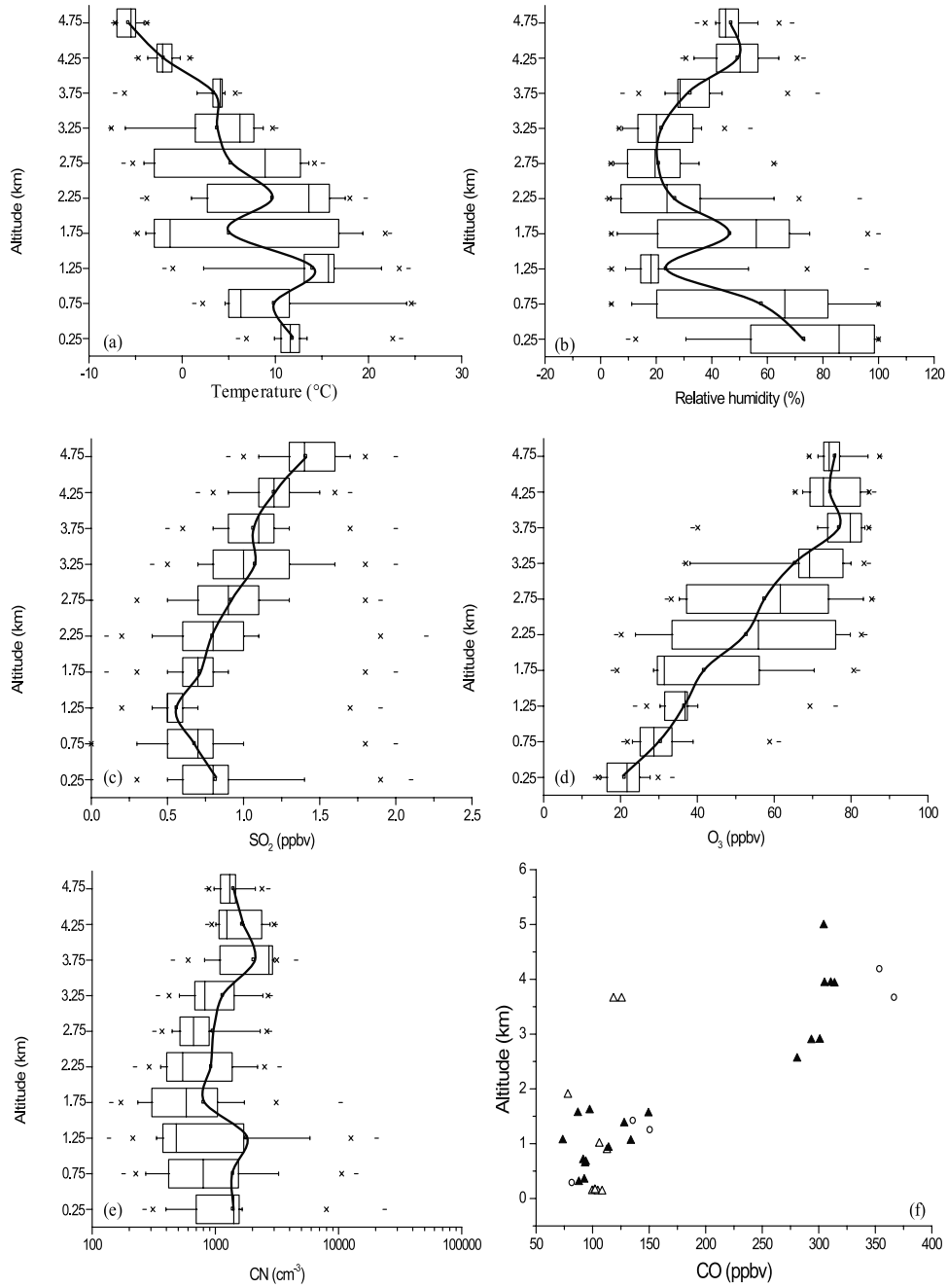

Figure 10. (a)–(e) As for Figure 6, but for vertical profiles 51–64 (from Table 1) over the Namibia sector for the period of September 10–16, 2000. (f) Intermittent samples of CO over the Namibia sector, with the open triangles indicating AFTIR measurements obtained on 14 September 2000, the closed triangles indicating AFTIR measurements obtained on 13 September 2000, and the circles indicating GC/C measurements obtained on 13 and 16 September 2000.

ranged from ~15–45%, increasing with increasing height above ~1.5 km.

[38] At the low relative humidities observed in the Botswana and Zambia sectors, the effect of RH on the aerosol light scattering coefficient is small [*Magi and Hobbs*, 2003]. The wide range of RH observed over the Namibia sector derives from differences in RH between the coastal and inland sampling locations. On average, RH in Namibia was highest below ~1 km (~60–75%) with a second peak at the ~1.75 km inversion layer and a third peak in the neutral layer above ~3.5 km. Outside of these layers, RH was low with median values of ~20%.

6.2. Sulfur Dioxide

[39] Vertical profiles of SO_2 over the South Africa, Mozambique, Botswana, Zambia, and Namibia sectors are summarized in Figures 6c–10c, respectively. The SO_2 mixing ratios over the South Africa sector (~2–25 ppbv; Figure 6c) are significantly higher than those typical for polluted continental air. The highest mixing ratios were

found near the surface, with a second peak about 1 km below the stable layer. The high mixing ratios of SO_2 near the surface suggest strong local sources, such as biomass burning (Figure 3), electric power generation plants, and mining operations. For example, the coal-burning electricity generation plants in the Mpumalanga province in northeastern South Africa emit significant quantities of SO_2. A typical emission factor for coal combustion is given by [*U.S. Environmental Protection Agency* (*U.S. EPA*), 1998]:

$$\text{Emitted } SO_2 \text{ (in g kg of fuel used)} = 19(\text{percentage of sulfur by weight in fuel}).$$

Since the percentage of sulfur by weight in South African coal is ~1% [*EIA*, 2002], the SO_2 emission factor is ~19 g per kg of fuel burned. This is about a factor of 45 greater than the SO_2 emission factor for savanna burning in southern Africa [*Sinha et al.*, 2003a].

[40] The SO_2 mixing ratios over the Mozambique sector ranged from ~0.5–6 ppbv (Figure 7c), comparable to values typical of polluted, continental air. Concentrations were lowest below ~1 km and around 2.75 km. Concentrations peaked at ~2 km; they were also high above ~3.25 km, where rapid removal by dry or wet deposition was not possible. The elevated SO_2 concentrations aloft suggest transport from the neighboring South Africa sector. The low SO_2 concentrations at ~2.75 km over the Mozambique sector were situated between two, polluted stable layers, suggesting the presence of what *Hobbs* [2002, 2003] called a "clean air slot," namely, a layer of clean, dry air a few hundred of meters thick sandwiched between layers of polluted air. Hobbs describes the presence of a clean air slot from ~2.5–3.4 km in the Mozambique sector at 0813–0815 UTC (Local time = UTC + 2 hr) on August 24, 2000. The average clean air slot seen in Figure 7c extends from ~2.5–3 km. On occasion, clean air slots were observed over South Africa and Namibia [*Hobbs*, 2002], but these are not apparent in the average profiles shown in Figures 6 and 10.

[41] Sulfur dioxide concentrations for the Botswana sector range from ~0.5–3 ppbv (Figure 8c), comparable to values typical for polluted, continental air. Concentrations peak in the mixed layer below the 2.5 km stable layer. With a lifetime at the surface of ~1 day due to dry deposition, the high SO_2 surface mixing ratios suggest local sources. Since there were few savanna fires within the region (Figure 3), the SO_2 peak near the surface most likely resulted from industrial sources. Botswana is one of the world's leading diamond producers, and two of Botswana's three largest diamond mines, the Letlhakane mine (21.42°S, 25.59°E) and the Orapa mine (21.28°S, 25.37°E), are located in the Botswana sector of this study (Mbendi, Information for Africa, 2003, available at http://www.mbendi.co.za/index.htm).

[42] Mixing ratios of SO_2 over the Zambia sector generally ranged from ~1–6 ppbv (Figure 9c), comparable to typical polluted continental concentrations. The SO_2 concentrations peaked below the stable layers at ~2.5 and ~4 km, with the highest concentrations around 3.25 km. The location of the SO_2 peak above the first stable layer suggests transport from another location.

[43] Over the Namibia sector, the average SO_2 concentrations below ~3 km were <1 ppbv (Figure 10c), with an average value of ~0.5 ppbv at ~1–1.5 km (close to the value of 0.2 ppbv typical for unpolluted air). Above ~3.5 km, where the atmosphere was neutral, the average SO_2 mixing ratios approached 1.5 ppbv, typical of polluted continental air. The high concentrations of SO_2 above ~3.5 km suggest transport from regions of heavy biomass burning in southern Angola (Figure 3). Removal of SO_2 by OH has a timescale of ~1 week, long enough to allow transport into the Namibia sector from Angola. Since the high SO_2 concentrations were located above both the cloud deck and the two stable layers, rapid SO_2 removal by dry or wet deposition was not possible.

6.3. Ozone

[44] Vertical profiles of O_3 over the South Africa, Mozambique, Botswana, Zambia, and Namibia sectors are summarized in Figures 6d–10d, respectively. The concentrations of O_3 for the South Africa sector (Figure 6d) ranged from ~35–80 ppbv, which is higher than those typical of remote locations (~20–40 ppbv) but lower than in aged smoke from savanna fires or polluted urban locations, which can exceed 100 ppbv. The O_3 concentrations in the South Africa sector generally increased with altitude, reaching peak values below the stable layer at ~3.5 km.

[45] Over the Mozambique sector, concentrations of O_3 below 1 km were <40 ppbv (Figure 7d), which is typical of remote locations. Above 1 km, the O_3 concentrations ranged from ~30–80 ppbv, with an average of ~70 ppbv above 3 km. As with the South Africa sector, the O_3 concentrations in the Mozambique sector were intermediate between those typical of remote locations and polluted urban air or biomass burning plumes. As in the case of the SO_2 profile, the O_3 minimum at ~2.75 km in the Mozambique sector suggests the presence of a clean air slot.

[46] Ozone concentrations in the Botswana sector range from ~50–110 ppbv (Figure 8d), which is comparable to O_3 concentrations in polluted urban areas and in aged smoke from savanna fires. The O_3 mixing ratios peak within the two stable layers from ~2.25–2.75 km and from ~3.25–4.25 km. The high O_3 concentrations aloft in the Botswana sector suggest the transport of emissions from surrounding regions of biomass burning (Figure 3). In fact, back trajectories indicate that air parcels in both stable layers were near ground level in central Zambia only 30–40 h earlier (HYbrid Single-Particle Lagrangian Integrated Trajectory (HYSPLIT) model, Air Resources Lab (ARL), National Oceanic and Atmospheric Administration (NOAA), 2002, available at www.arl.noaa.gov/ready/hysplit4.html).

[47] Ozone concentrations in the Zambia sector generally ranged from ~60–110 ppbv (Figure 9d), again typical of polluted urban environments and biomass burning plumes. The concentrations of O_3 in the Zambia sector increased with increasing altitude up to ~2.5 km, above which they were fairly uniform and typically above ~80 ppbv. Ozone concentrations peaked to average values of ~95 and 110 ppbv around the stable layers at ~2.5 and ~4 km, respectively. Since there was considerable biomass burning in the Zambia sector, and it was surrounded by regions of intense biomass burning (Figure 3), the high O_3 concentrations aloft in this sector probably resulted from net ozone production in both local and aged transported biomass smoke.

[48] Below ~1.5 km over the Namibia sector, the O_3 mixing ratios ranged from ~15–40 ppbv (Figure 10d),

which is typical of remote locations. The O_3 concentrations increased with increasing height, stabilizing at ~80 ppbv in the neutral layer above ~3.5 km. This peak O_3 concentration over Namibia is comparable to that in polluted, urban air and in smoke plumes from savanna fires. As with SO_2, the source of O_3 aloft over Namibia was probably intense biomass burning to the north and northeast (Figure 3).

6.4. Condensation Nuclei

[49] Figures 6e–10e summarize the vertical profiles of CN over the South Africa, Mozambique, Botswana, Zambia, and Namibia sectors, respectively. Over the South Africa sector, there was a relatively uniform concentration of CN up to the stable layer at 3.5 km, followed by a sharp decrease above this level (Figure 6e). The CN concentrations ranged from ~200–20,000 cm^{-3}, with the variance in the concentrations increasing with increasing altitude. The range in CN concentrations over the South Africa sector overlaps with the lower end of the ~10,000–400,000 cm^{-3} range typically found at polluted, continental sites. The electric generation plants in northeast South Africa burn coal with a high (45%) ash content [*EIA*, 2002], which may contribute to the high CN concentrations in this sector.

[50] Concentrations of CN in the Mozambique sector ranged from ~200–8,000 cm^{-3} (Figure 7e), compared to ~50–10,000 cm^{-3} typically found over remote, continental locations, and ~100–400 cm^{-3} typically found over marine locations. At 2.75 km, where minima were present in SO_2 and O_3 concentrations, the median CN concentration over the Mozambique sector was only ~700 cm^{-3}, the lowest at any altitude in the profile, and typical of clean continental air. The relatively low concentrations of particles at 2.75 km over Mozambique, combined with the low relative humidity and SO_2 and O_3 concentrations (Figure 7), confirm the presence of a clean air slot at this altitude.

[51] Below ~4 km over the Botswana sector, the CN concentrations were fairly uniform with height, ranging from ~2,000–10,000 cm^{-3} (Figure 8e), which is similar to the range typically found over rural, continental locations. Concentrations were highest in the mixed layer below the ~2.5 km stable layer. Above ~4 km, the CN concentration in the Botswana sector decreased. The high CN concentrations lower down could have been due in part to emissions from operations associated with diamond mines.

[52] The CN concentrations in the Zambia sector ranged from ~2,000–10,000 particles cm^{-3} (Figure 9e), which is similar to those found in rural, continental sites. The CN concentrations decreased with increasing height, with a local minimum near the ~2.5 km stable layer. The high CN concentrations seen throughout the vertical profile indicate a deep polluted layer to an altitude of at least 5 km. Light-scattering and light-absorption measurements obtained within the Zambia sector from 0746–0755 UTC on September 6, 2000, show a deep polluted layer extending above 5 km and nearly reaching the 500 hPa pressure level [*Magi et al.*, 2003; *Schmid et al.*, 2003].

[53] The measured CN concentrations over the Namibia sector varied from ~200–6,000 cm^{-3} (Figure 10e), compared to ~50–10,000 cm^{-3} over remote, continental locations and ~100–400 cm^{-3} typically found over the oceans. The CN concentrations over Namibia peaked at the first stable layer at ~1.25 km, and again at ~3.75 km in the neutral layer.

6.5. Intermittent Samples of Carbon Monoxide

[54] Measurements of CO through grab samples of ambient air away from visible plumes were obtained by two independent methods: gas chromatography on 38 canister samples (GC/C), and IR spectroscopy on 203 samples temporarily detained within the AFTIR cell (see section 2). From these data, vertical profiles of CO were constructed for the five sectors, as shown in Figures 6f–10f.

[55] Of the five sectors, CO concentrations over the Zambia sector were the highest on average, with mixing ratios from ~250–650 ppbv (Figure 9f); this is substantially higher than those typical of remote regions (~50–150 ppbv). Since there are few industrial sources of CO in the Zambia sector, the high CO values suggest that biomass burning was the primary source. This is consistent with the fact that the concentrations of CO measured in the Zambia sector almost doubled as the river-of-smoke became increasingly developed. The Zambia sector also had high concentrations of O_3 and CN (Figure 9), which are also indicators of smoke from biomass fires.

[56] The second highest average concentrations of CO were over the Botswana sector, where they ranged from ~150–550 ppbv below ~3 km but decreased at higher altitudes (Figure 8f). Again, these CO mixing ratios are substantially greater than those typical of remote regions (~50–150 ppbv). Since there were relatively few savanna fires in this sector (Figure 3), the high CO concentrations likely resulted from smoke from biomass burning being transported into the sector from surrounding regions of intense savanna burning. This is again consistent with an approximate doubling of the CO concentrations in Botswana as the river-of-smoke transported increasing amounts of smoke from the north. Mining operations within the Botswana sector could also have contributed to the CO. On one occasion in this sector, we observed a stable layer "break up" during the day and release the CO trapped below it.

[57] The CO concentrations in the South Africa sector ranged from ~50–250 ppbv (Figure 6f), significantly lower than those in the Zambia and Botswana sectors. This, together with the moderate O_3 concentrations in the South Africa sector (Figure 6d), suggest that this sector was not affected by biomass burning smoke as much as the Zambia and Botswana sectors. In addition, the CO mixing ratios in the South Africa sector never exceeded 150 ppb above 4 km, except for one sample obtained within a high cumulus cloud [*Yokelson et al.*, 2003].

[58] The CO concentrations over the Mozambique sector ranged from ~130–210 ppbv (Figure 7f). These concentrations are comparable to those over the South Africa sector, which suggests that both sectors were similarly affected by emissions from biomass burning. In Mozambique, the near-surface CO concentrations were higher over land than just offshore. The highest CO concentration measured offshore was near the top of the first inversion at ~1.25 km, while the highest CO concentration measured over the land was near the top of the third inversion at ~2.75 km. This difference could be due to the fact that the measurements

over land were obtained later in the day and over a warmer surface than over the ocean.

[59] The CO concentrations below ~2 km over the Namibia sector ranged from ~50–150 ppbv (Figure 10f), which is typical for remote regions. The concentrations of SO_2, O_3, and CN were also low below ~2 km in the Namibia sector. However, above ~2 km and in the vicinity of 21°S, the CO concentrations in the Namibia sector ranged from ~275–375 ppbv, which are greater than the CO concentrations in the South Africa sector and approach those over the Zambia and Botswana sectors. We attribute the high concentrations of CO, as well as O_3 and SO_2 (Figure 10), aloft in the northern part of the Namibia sector to the transport of biomass smoke from the regions of heavy biomass burning to the north and northeast of Namibia (Figure 3). This is confirmed by HYSPLIT back trajectories (section 7). On 13 September 2000, polluted air aloft at 21°S over Namibia had been over southern Angola 5 days earlier, while the air at the same altitude sampled at 26°S over Namibia on 14 September 2000 had passed over the Antarctic Ocean 5 days earlier. On both days, the lower, cleaner layer was transported from the remote south Atlantic Ocean.

7. Air Mass Trajectories

[60] The HYSPLIT software was used to obtain five-day forward and five-day back air mass trajectories for each of the profiles listed in Table 1. The dates, times, and altitudes in Table 1 were used to initialize the trajectory runs, with the back trajectories beginning, and the forward trajectories ending, at the center of the altitude range for a given sample profile. Additional trajectories were initialized at the top of the altitude range for a given sample profile. Since these trajectories were generally similar to those initialized at the center of the altitude range for a sample profile, only the latter are discussed here. A schematic illustrating the results of the back and forward trajectories obtained is shown in Figures 11a and 11b, respectively, and is discussed below.

7.1. South Africa Sector

[61] The back trajectories for the South Africa sector show that about three quarters of the air parcels came from the southeast over the Indian Ocean, corresponding to the southeasterly trade winds, and about a quarter of the trajectories came from the south, passing over areas of savanna burning (Figure 3). Since the majority of the back trajectories came from unpolluted areas, the source of the high SO_2 mixing ratios at low altitudes over the South Africa sector (Figure 6b) most likely derived from industries and biomass burning within that sector.

[62] Forward trajectories for the South Africa sector show that about 80% of the air parcels exited the continent toward the Indian Ocean. The remaining 20% headed westward toward the Namibia sector. It should be noted that most of the profiles over the South Africa sector (Table 1) were obtained in August 2000, prior to the river-of-smoke episode. Therefore, the trajectories generally correspond to the average climatology of the region during the dry season, as depicted in Figure 4a.

7.2. Mozambique Sector

[63] Back trajectories for the Mozambique sector show that the air parcels that entered this sector were about evenly

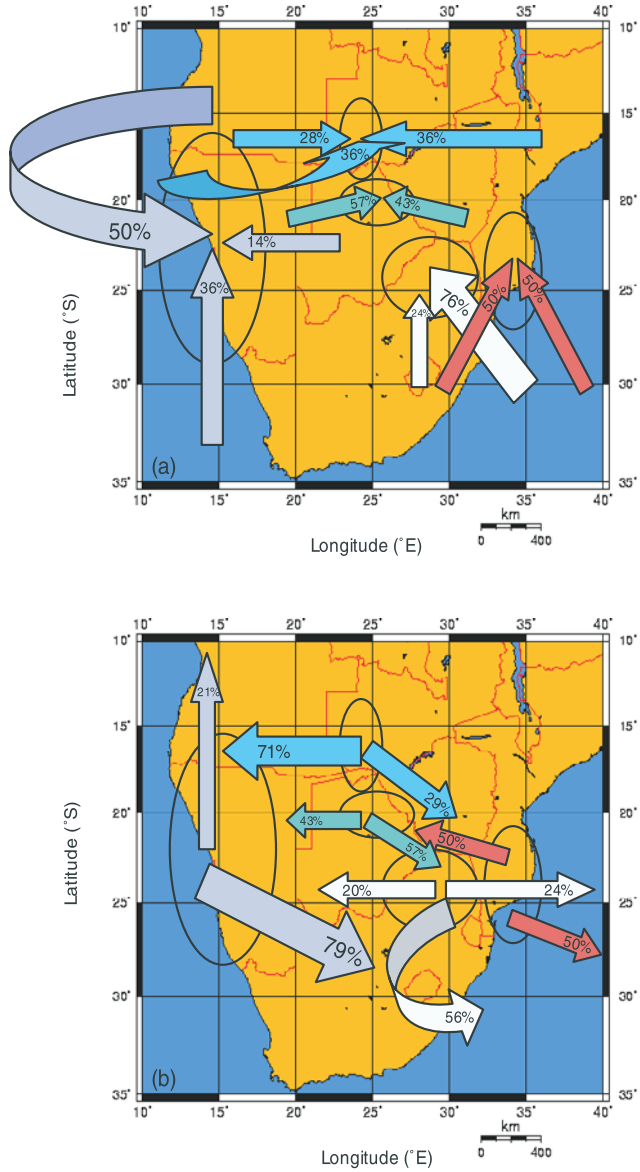

Figure 11. Schematic of 5 day (a) back trajectories, and (b) forward trajectories for the South Africa sector (white arrows), Mozambique sector (red arrows), Botswana sector (green arrows), Zambia sector (blue arrows), and Namibia sector (violet arrows). The ovals show the locations of the five sectors. The percentages refer to the fraction of the trajectories that followed the indicated path. One back and one forward trajectory were obtained for each of the vertical profiles listed in Table 1. The dates, times, and altitudes in Table 1 were used to initialize the trajectory runs, with the back trajectories beginning, and the forward trajectories ending, at the center of the altitude range for each profile.

divided between southeasterly and southwesterly approaches. The southwesterly trajectories passed over abundant savanna fires in northeast South Africa, thereby transporting aged smoke, enhanced in secondary pollutants such as organic acids and O_3, to the Mozambique sector [*Hobbs et al.*, 2003]. These products likely contributed to the high O_3 concentrations above ~3 km in the Mozambique sector (Figure 7c). The southeasterly trajectories, cor-

responding to the general trade wind circulation, passed over the Indian Ocean, bringing generally clean air to the Mozambique sector.

[64] About half of the forward trajectories for the Mozambique sector show westward transport that follows the general subcontinental gyre (Figure 4a), which transported aged smoke from Mozambique to Botswana. The remaining trajectories show transport eastward, exiting the continent over the coast of the Indian Ocean.

7.3. Botswana Sector

[65] Back trajectories for the Botswana sector show air parcels nearly evenly divided between easterly and westerly approaches. Both approaches transported smoke from surrounding areas of intense biomass burning (Figure 3). The profiles for the Botswana sector (Table 1) were obtained during the transition into the river-of-smoke episode of early September 2000. Therefore, the trajectories for this sector reflect a combination of the typical dry season climatology depicted in Figure 4a and the flow that gave rise to the river-of-smoke perturbation shown in Figure 4b. Forward trajectories for the Botswana sector are nearly evenly divided between eastward trajectories heading toward the Indian Ocean and westward trajectories heading for the Atlantic Ocean.

7.4. Zambia Sector

[66] Back trajectories for the Zambia sector show air parcels nearly evenly divided between southwesterly, westerly and easterly approaches. In view of the abundance of savanna fires to the south, west and east of the Zambia sector (Figure 3), these back trajectories suggest that the impact of local burning in the Zambia sector was augmented by smoke from biomass burning in surrounding regions.

[67] Forward trajectories for this sector show the majority of the parcels following the general trade wind circulation, exiting westward toward the Atlantic Ocean where they contribute to the O_3 anomaly over the southern Atlantic. The remainder of the parcels travel southeastward into South Africa.

[68] Many of the profiles for the Zambia sector (Table 1) were obtained during the river-of-smoke episode in early September 2000. Therefore, the trajectories for this sector are a combination of those typical of the dry season climatology depicted in Figure 4a and the river-of-smoke perturbation shown in Figure 4b. The deep polluted layer over this sector (Figure 9) can be attributed to the river-of-smoke perturbation.

7.5. Namibia Sector

[69] Back trajectories over the Namibia sector show about half the parcels originating over the heavy savanna burning region of Angola, exiting the continent over the Atlantic coast, and then returning to the continent over Namibia. About a third of the back trajectories passed over clean areas to the south of Namibia. The O_3 in the upper polluted layer over the Namibia sector is due to photochemistry in aging biomass burning emissions. *Hobbs et al.* [2003] showed that net O_3 production can occur in biomass burning plumes within ~10 minutes. Production of O_3 in biomass plumes has been observed to continue for at least 10 days [*Andreae et al.*, 1994]

[70] Forward trajectories for the Namibia sector show most of the air parcels heading southeastward, eventually passing over the Indian Ocean. Since our measurements over Namibia were obtained during September, a month of frequent penetrations by frontal perturbations and unstable air masses, the trajectories resemble a combination of the typical dry season climatology depicted in Figure 4a and the river-of-smoke perturbation shown in Figure 4b.

8. Comparisons of Vertical Profiles With Other Studies

[71] The SAFARI-92 project, which took place in September and October 1992, investigated pyrogenic emissions in southern Africa. Using measurements from ozonesonde launches from Ascension Island, Brazzaville, Okakuejo, and Irene, *Diab et al.* [1996] characterized the vertical distribution of ozone in southern Africa. Irene (25.87°S, 28.22°E) is located within the South Africa sector of the present study, while Okaukuejo (19.18°S,15.92°E) is within the Namibia sector. Diab et al. reported O_3 (1 σ) concentration ranges of ~25–55 ppbv at an altitude of 2 km and ~50–65 ppbv at an altitude of 4 km over Irene. Our corresponding O_3 (1 σ) concentrations for the South Africa sector range from ~37–65 ppbv just below 2 km and ~54–74 ppbv just below 4 km. In both the Irene profile and our South Africa sector profile, the O_3 concentrations increase, on average, with increasing altitude. Over Okakuejo, Diab et al. report O_3 (1 σ) concentration ranges of ~40–70 ppbv at 2 km and ~45–75 ppbv at 4 km. Our corresponding O_3 (1 σ) concentrations for the Namibia sector are ~25–59 ppbv just below 2 km, and 68–86 ppbv just below 4 km. While both studies show increasing O_3 with increasing altitude in Namibia, our measurements at 21°S show a more pronounced increase in O_3 with increasing altitude.

[72] The TRACE A experiment, which took place in September and October 1992, investigated the effects on the tropical South Atlantic troposphere of biomass burning emissions in the dry season from South America and southern Africa. *Blake et al.* [1996] describe vertical profiles of CO over northeastern Zambia (9.8–11.4°S, 29.0–30.6°W) and western Zimbabwe (18.2–19.0°S, 26.2–27.4°W), near the Zambia and Botswana sectors of the present study. Below 5 km, Blake et al. report CO concentrations ranging from ~100 to 700 ppbv, with the majority between ~200–500 ppbv. Above 5 km, the CO concentrations decreased to a uniform value of ~100 ppbv. In the present study, CO concentrations below 5 km over the Botswana and Zambia sectors range from ~150–650 ppbv (Figures 8f–9f).

[73] *Thompson et al.* [2002] describe O_3 profiles obtained from soundings launched from Lusaka, Zambia (15.5°S, 28.0°E) and Irene, South Africa (25.87°S, 28.22°E) in August and September 2000, the same time period as the present study. The Lusaka soundings show O_3 concentrations of ~50–100 ppbv below 2.5 km, and >100 ppbv from 2.5–5 km. Our study shows O_3 concentrations in the Zambia sector, located to the west of Lusaka, of ~60–90 ppbv below 2.5 km and ~70–110 ppbv from 2.5–5 km (Figure 9d). A sounding over Irene, located within the South Africa sector, shows O_3 concentrations of ~50–70 ppbv below 5 km. Our study shows O_3 concentrations in the South Africa sector of ~30–80 ppbv below 5 km (Figure 6d).

[74] Outside of Africa, significant biomass burning in the tropics occurs in Brazil and Indonesia. For the SCAR-B

Table 2. Average Background Concentrations Below 5 km msl of Selected Gaseous and Particulate Species Over Five Sectors in Southern Africa During the Period August 14 to September 16, 2000[a]

Species[b]	Units	Measurement Technique[c]	South Africa Sector (29.15°E, 23.99°S)		Mozambique Sector (32.79°E, 26.10°S)		Botswana Sector (26.29°E, 20.68°S)		Zambia Sector (24.00°E, 15.98°S)		Namibia Sector (14.20°E, 19.89°S)		All Sectors Average
			Average	n	Average	n	Average	n	Average	n	Average	n	
CO_2	ppmv	GC/C, AFTIR	387 ± 12	102	384 ± 7	7	388 ± 7	22	392 ± 6	36	381 ± 6	34	386 ± 8
CO	ppbv	GC/C, AFTIR	157 ± 47	102	165 ± 43	15	369 ± 120	22	453 ± 101	36	162 ± 96	34	261 ± 81
CH_4	ppbv	GC/C, AFTIR	1736 ± 41	72	1710 ± 55	7	1753 ± 12	22	1758 ± 28	36	1718 ± 32	34	1735 ± 21
Ethane	pptv	GC/C	857 ± 442	18	428	1	1268 ± 442	5	1532 ± 642	2	715 ± 397	5	960 ± 440
Ethene	pptv	GC/C	138 ± 107	18	137	1	320 ± 226	5	271 ± 112	2	35 ± 27	5	180 ± 115
Propane	pptv	GC/C	123 ± 72	18	69	1	216 ± 34	5	188 ± 73	2	67 ± 32	5	133 ± 68
Alkenes ($\geq C_3$)	pptv	GC/C	35 ± 21	18	19	1	33 ± 12	5	34 ± 15	2	12 ± 5	5	27 ± 10
Alkanes ($\geq C_4$)	pptv	GC/C	87 ± 39	18	65	1	87 ± 46	5	60 ± 20	2	24 ± 11	5	65 ± 26
Isoprene	pptv	GC/C	8 ± 9	18	8	1	19 ± 15	5	12 ± 7	2	4 ± 2	5	10 ± 6
SO_2	ppbv	Teco 43S	5.1 ± 2.4	25	2.9 ± 2	4	1.7 ± 0.3	7	2.2 ± 0.7	14	0.8 ± 0.3	14	2.5 ± 1.6
O_3	ppbv	Teco 49C	54 ± 11	25	51 ± 14	4	79 ± 12	7	88 ± 12	14	50 ± 16	14	64 ± 13
CH_3Br	pptv	GC/C	9 ± 1	18	8	1	10 ± 1	5	9 ± 1	2	9 ± 1	5	9 ± 1
CH_3Cl	pptv	GC/C	634 ± 72	18	575	1	688 ± 60	5	690 ± 48	2	580 ± 60	5	633 ± 56
CN	cm^{-3}	TSI 3025A	$(6.4 \pm 5.2) \times 10^3$	25	$(3.4 \pm 2.5) \times 10^3$	4	$(3.5 \pm 0.8) \times 10^3$	7	$(5.9 \pm 1.5) \times 10^3$	14	$(1.0 \pm 0.6) \times 10^3$	14	$(4.5 \pm 2.9) \times 10^3$
Total particle mass	$\mu g/m^3$	Gravimetric/Filter	29.6 ± 14.6	16	31.2 ± 23.5	2	20.1 ± 15.0	12	22.3 ± 4.2	4	26.8	1	26.0 ± 4.7
Organic acids	$\mu g/m^3$	IC/Filter	0.6 ± 0.4	16	1.4 ± 1.2	2	1.0 ± 1.0	12	1.0 ± 0.7	4	1.7	1	1.1 ± 0.4
Sulfate	$\mu g/m^3$	IC/Filter	8.3 ± 8.1	16	8.5 ± 5.0	2	1.9 ± 1.5	12	0.9 ± 0.1	4	2.8	1	4.5 ± 3.6
Nitrate	$\mu g/m^3$	IC/Filter	0.3 ± 0.2	16	0.8 ± 0.3	2	1.0 ± 1.0	12	0.9 ± 0.1	4	0.8	1	0.8 ± 0.3
Potassium	$\mu g/m^3$	PAES/Filter	0.3 ± 0.2	16	0.5 ± 0.5	2	0.4 ± 0.4	12	0.2 ± 0.1	4	0.5	1	0.4 ± 0.1
Black carbon (BC)	$\mu g/m^3$	ATN/Filter	1.1 ± 0.4	17	1.0 ± 0.5	2	2.6 ± 1.4	11	5.5 ± 1.4	4	1.0	1	2.3 ± 1.9
Total carbon (TC)	$\mu g/m^3$	EGA/Filter	4.8 ± 1.7	6	5.9 ± 5.1	2	13.2 ± 6.8	11	14.3	1	4.4	1	8.5 ± 4.8
BC/TC	—	—	0.23	—	0.17	—	0.20	—	0.38	—	0.23	—	0.27
Potassium/BC	—	—	0.27	—	0.50	—	0.15	—	0.04	—	0.50	—	0.17

[a]Here n is the number of samples.
[b]Beginning with "total particle mass," the concentrations refer to particles with diameter <3 μm.
[c]GC/C, gas chromatography via canisters; ATN/Filter, optical attenuation via filters; EGA/Filter, evolved gas analysis via filters; IC, ion chromatography via filters; PAES/Filter, plasma-emission spectrometry via filters.

campaign in August–September 1995, *Reid et al.* [1998] reported average CO and O_3 concentrations of ~500–800 ppbv and ~60–100 ppbv, respectively, below 4 km in regional hazes dominated by emissions from the burning of cerrado and rain-forested regions in Brazil. Average CO and O_3 concentrations below 4 km in the present study range from ~150–450 ppbv and ~50–90 ppbv, respectively. During the PACE-5 campaign in October of 1997, *Sawa et al.* [1999] measured CO concentrations of 3 to 9 ppm below 3 km in thick smoke haze over Kalimantan, Indonesia. These CO concentrations are an order of magnitude greater than those measured by us over southern Africa. The high CO concentrations over Indonesia resulted from extensive forest fires during a long drought associated with a strong El Nino event.

9. Horizontal Distributions

[75] In addition to characterizing the vertical distribution of selected pollutants, the horizontal distributions of a larger set of pollutants were measured from the UW Convair-580 aircraft over southern Africa during the dry biomass burning season in SAFARI 2000. Table 2 lists the measured average concentrations of twenty gaseous and particulate species below an altitude of 5 km during the period August 14 to September 16, 2000 in the five sectors defined in section 3. The species include long-lived gases (such as CO_2, CO, and CH_4), shorter-lived gases (such as SO_2, O_3, and various nonmethane hydrocarbons), halocarbons, carbonaceous and inorganic particulate species, and CN. These species play important roles in global atmospheric chemistry and the earth's radiative balance. The results are summarized below.

9.1. Carbon Dioxide, Methane, and Carbon Monoxide

[76] Carbon dioxide, CH_4, and CO are long-lived emission products of biomass burning and other types of combustion. Globally averaged background concentrations of CO_2 and CH_4 in 2000 were ~367 ppmv and ~1.750 ppmv, respectively [*Intergovernmental Panel on Climate Change* (*IPCC*), 2001]. The typical background concentration of CO in unpolluted areas is ~40–200 ppbv [*Seinfeld and Pandis*, 1998]. Of the five sectors in this study, the Zambia and Botswana sectors had the highest mixing ratios of these gases (~390 ppmv of CO_2, ~1.75–1.76 ppmv of CH_4, and ~370–450 ppbv of CO) (Table 2). There are relatively few industries in the Zambia and Botswana sectors, but there is abundant biomass burning in Zambia. Both sectors are susceptible to smoke transported from intense biomass burning in Angola, Zimbabwe, Mozambique, and South Africa (Figure 3). Since CO and CH_4 are the dominant sinks for the OH radical [*Hobbs*, 2000], high concentrations of CO and CH_4 will perturb the oxidative capacity of the troposphere in the Zambia and Botswana sectors.

9.2. Nonmethane Hydrocarbons

[77] Nonmethane hydrocarbons are important emission products of biomass burning. Since the lifetime of alkanes in the tropics is on the order of days but the lifetime of alkenes is on the order of hours [*Mauzerall et al.*, 1998; *Hobbs et al.*, 2003], the presence of high concentrations of alkenes suggests local sources, whereas, high concentrations of alkanes could also result from longer range transport.

[78] The Botswana and Zambia sectors had significantly higher concentrations of ethane, ethene, and propane than the other five sectors. *Reid et al.* [1998] reported high alkane concentrations in regional hazes in Brazil (e.g., ethane from 7–11 ppbv). The high alkane levels in Brazil, Botswana, and Zambia could be due to a larger proportion of woody fuels [*Bertschi et al.*, 2003b].

[79] Nonmethane hydrocarbons play an important role in atmospheric photochemistry. Oxidation of organic compounds (including hydrocarbons) in the presence of nitrogen oxides leads to formation of O_3. For example, in NO_x-rich, young biomass burning plumes, oxidation of nonmethane organic compounds (NMOC, of which ~30% are hydrocarbons) leads to rapid formation of O_3. In the plume from the Timbavati fire, discussed in section 5, O_3 mixing ratios exceeded 100 ppbv after only ~30 minutes of plume aging [*Hobbs et al.*, 2003]. However, since the lifetime of NO_x is short (~1 day) [*Hobbs*, 2000], NO_x concentrations in the background troposphere over southern Africa are low and dominated by the recycling of NO_x from its oxidation products [*Jacob et al.*, 1996]. In a low NO_x environment, oxidation of CO and NMOC will diminish the concentration of the OH radical. Alkanes are primarily oxidized by the OH radical, whereas, alkenes can also be oxidized by O_3.

[80] Isoprene, which is a by-product of photosynthesis, is the dominant compound emitted by vegetation. With a lifetime of ~1 h, isoprene is quickly oxidized by OH [*Seinfeld and Pandis*, 1998]. In the presence of NO_x, isoprene oxidation results in rapid O_3 formation. However, in a low NO_x environment, isoprene serves as an overall sink for OH. Over the five sectors of the present study, isoprene concentrations were fairly low, ranging from <3 to ~35 pptv (Table 2). Isoprene concentrations were highest in the Botswana and Zambia sectors, and lowest in the extremely arid Namibia sector.

9.3. Sulfur Dioxide and Ozone

[81] Except for the Namibia sector, average SO_2 concentrations in this study (~1.5–5 ppbv; Table 2) were equal to or exceeded the value of ~1.5 ppbv, which is typical of polluted, continental air. The highest average SO_2 concentration was over the South Africa sector (5.1 ± 2.4 ppbv), which was likely due to those coal-burning, electric generation plants and mining operations in northeast South Africa that do not employ pollution controls, and the numerous savanna fires in this sector (Figure 3). The average SO_2 concentration in the Namibia sector was 0.8 ± 0.3 ppbv (Table 2), which is still considerably greater than that typical of clean continental air (~0.2 ppbv).

[82] Ozone concentrations in all five sectors of this study (~40–100 ppbv; Table 2) exceeded the range of ~20–40 ppbv typical of remote locations. This is attributable to extensive biomass burning throughout southern Africa during the dry season (Figure 3) and the photochemical transformation/transport of these emissions throughout the region. Ozone concentrations were highest in the Zambia and Botswana sectors (88 ± 12 and 79 ± 12 ppbv, respectively); these values are comparable to those typical of polluted, urban air. We attribute the high concentrations in the Zambia and Botswana sectors to biomass burning in Zambia, and the transport of smoke to these sectors from Angola, Zimbabwe, South Africa, and Mozambique.

9.4. Methyl Halides

[83] Halogens in the stratosphere are efficient at catalyzing the rapid destruction of stratospheric ozone; sufficient quantities of methyl halides are emitted by biomass burning to play a role in stratospheric ozone loss [*Mano and Andreae*, 1994]. Due to their long lifetimes (~1 year), methyl halides are fairly well mixed in the troposphere. Average concentrations of methyl chloride for the five sectors in this study ranged from ~575 pptv to 690 pptv (Table 2); typical continental background concentrations are ~600 pptv [*Seinfeld and Pandis*, 1998]. The average concentrations of methyl bromide ranged from ~8 pptv to 10 pptv over the five sectors (Table 2), compared to typical background continental concentrations in the southern hemisphere of ~7–8 pptv [*Wingenter et al.*, 1998].

9.5. Total Particle Mass

[84] Total particle mass is often dominated by particles with diameters >1 μm [*Hobbs*, 2000]. These large particles (e.g., dust, pollen, sea-salt) are often generated by natural, mechanical processes. Typical background concentrations of total particle mass are ~5 μg m^{-3} in remote locations, ~15 μg m^{-3} in rural continental air, and ~32 μg m^{-3} in urban air [*Seinfeld and Pandis*, 1998]. The average total particle mass over the five sectors in this study ranged from ~20–30 μg m^{-3}, which approaches that in polluted, urban air.

9.6. Condensation Nuclei

[85] Condensation nucleus concentrations are dominated by particles with diameters <1 μm. Since most of the particles generated by combustion processes have diameters <1 μm, sub-micron particles from combustion should affect the distribution of CN concentrations over southern Africa. In this study, the concentration of CN was, on average, greatest over the South Africa sector (6400 ± 5200 cm^{-3}; Table 2) where it overlapped with the range typical of polluted, continental locations (10,000 cm^{-3} to 400,000 cm^{-3}). Again, we attribute this to the extensive biomass burning (Figure 3) and mining and electric generation operations in the South Africa sector (section 5). The sector with the lowest average concentration of CN was Namibia (1000 ± 600 cm^{-3}).

9.7. Carbonaceous Particles

[86] Carbonaceous particles are composed of black (elemental) carbon and organic carbon. They derive from primary pyrogenic and biogenic emissions and secondary low vapor pressure products of oxidation of organic gases.

[87] Black carbon is produced only by combustion processes; it is the primary light-absorbing aerosol species in the atmosphere. Typical background concentrations of black carbon are ~0.2–2.0 μg m^{-3} in rural and remote continental air, and 1.5–20 μg m^{-3} in urban air [*Seinfeld and Pandis*, 1998]. In this study, black carbon concentrations were highest over the Zambia and Botswana sectors (5.5 ± 1.4 and 2.6 ± 1.4 μg m^{-3}, respectively; Table 2), comparable to values in urban air. The concentrations of black carbon in the other three sectors (~0.5–1.5 μg m^{-3}) were within the range typical of rural and remote continental air.

[88] Organic carbon comprises a large and varied class of compounds, including n-alkanes, organic acids, and aromatic species. Unlike black carbon, organic particles tend to scatter solar radiation rather than absorb it. Typical concentrations of organic carbon range from ~4.2–5.6 μg m^{-3} in rural, continental areas to ~6–32 μg m^{-3} in polluted, continental areas [*Seinfeld and Pandis*, 1998]. Concentrations of organic carbon were obtained in the present study by subtracting the measured concentrations of black carbon from those of total carbon (Table 2). The concentrations of organic carbon in the Zambia and Botswana sectors (~8.8 and 10.6 μg m^{-3}, respectively) are comparable to the concentrations present in polluted continental locations. The concentrations of organic carbon in the South Africa, Mozambique, and Namibia sectors (~3–5 μg m^{-3}) lie within the range typical of rural sites.

[89] Samples obtained above and downwind of the Timbavati fire showed that particulate organic acids are generated both directly from savanna burning and by the oxidation of NMOC released from savanna fires and subsequent gas-to-particle conversion [*Gao et al.*, 2003]. Concentrations of organic acids were <2 μg m^{-3} and fairly uniform throughout the five sectors (Table 2).

[90] The average concentration of carbonaceous particles (black carbon plus organic carbon) was highest in the Botswana and Zambia sectors (~13–14 μg m^{-3}; Table 2), likely due to the emissions from biomass burning. The mass fraction of carbonaceous particles to total particle mass was also highest in the Botswana and Zambia sectors (~65%).

[91] The mass ratio of black carbon to total carbonaceous particles typically ranges from ~0.15–0.20 in rural areas to ~0.2–0.6 in urban areas [*Seinfeld and Pandis*, 1998]. In this study, the ratios of black carbon mass to total carbonaceous particle mass ranged from ~0.18 to 0.40 (Table 2), which is comparable to the range in urban environments. Again, this indicates the strong influence of biomass burning on particle properties over southern Africa.

[92] The origin of the high carbonaceous aerosol content over the Zambia sector requires further discussion. The ratios of black carbon to total carbon (BC/TC), black carbon to organic carbon (BC/OC), and potassium to black carbon (K/BC) are ~0.38, 0.63, and 0.04, respectively, for this sector. These ratios differ from those obtained from savanna burning source characterization studies (~0.13, 0.14, 0.71, respectively [*Andreae and Merlet*, 2001]), but they are similar to those found in urban environments dominated by fossil fuel burning (BC/TC of ~0.2–0.6, BC/OC of ~0.25–1.5 [*Seinfeld and Pandis*, 1998], and K/BC of ~0.025–0.09 [*Andreae*, 1983]). Although there are few industrial sources of pollution within the Zambia sector of this study, the heavy mining and development activities of the "copper belt" north of the Zambia sector may contribute carbonaceous aerosol to this sector.

9.8. Inorganic Particles

[93] Like organic particles, inorganic particles tend to scatter solar radiation rather than absorb it. Sulfates and nitrates also affect the acidity of the troposphere. Background concentrations of sulfate typically range from ~0.5–2 μg m^{-3} in unpolluted continental air, >10 μg m^{-3} in urban air, and ~3 μg m^{-3} in marine air [*Warneck*, 2000]. In this study, sulfate concentrations were highest over the South Africa and Mozambique sectors (8.27 ± 8.06 and 8.48 ± 5.01, respectively; Table 2), where they approached those typical of polluted urban air. The many coal-burning

electric generation plants and mining operations in northeast South Africa, and extensive biomass burning in the South Africa and Mozambique sectors, were no doubt responsible for the high sulfate concentrations. Sulfate concentrations in the Botswana, Zambia, and Namibia sectors were <3 $\mu g\ m^{-3}$.

[94] Nitrate is a common component of tropospheric aerosols. It is produced by the oxidation of NO_2 by OH or O_3 to eventually form HNO_3. Typical background concentrations of nitrate range from ~0.4–1.3 $\mu g\ m^{-3}$ in unpolluted continental air, 3–10 $\mu g\ m^{-3}$ in urban air, and <0.1 $\mu g\ m^{-3}$ over oceans [*Warneck*, 2000]. In this study, nitrate concentrations were low and fairly uniform over the five sectors (<2 $\mu g\ m^{-3}$; Table 2), which places them in the range of unpolluted continental air. However, the air was, in fact, polluted, but biomass combustion occurs below the threshold for thermal NO_x formation and thus it is often a "low-nitrate" pollution source.

[95] Potassium has been used as an indicator of smoke from savanna burning [*Cachier et al.*, 1995]. Background concentrations of total particulate potassium range from ~0.03–0.12 $\mu g\ m^{-3}$ in unpolluted continental air, ~0.4–0.9 $\mu g\ m^{-3}$ in urban air, and ~0.1 $\mu g\ m^{-3}$ in marine air [*Warneck*, 2000]. Due to extensive biomass burning in southern Africa during the dry season (Figure 3), the average particulate potassium concentrations in this study (~0.3–0.5 $\mu g\ m^{-3}$; Table 2) were comparable to the range typical of polluted urban air.

9.9. Average Pollutant Concentrations Over All Sectors

[96] The average concentration of a pollutant over all five sectors in this study provides an estimate of the concentration of that pollutant below an altitude of ~5 km in southern Africa from August 14 to September 16 during the dry biomass burning season of 2000. These average concentrations are listed in the last column of Table 2. With the exception of the South Africa and Botswana sectors, the measurements in this study were obtained in locations that have few local sources of industrial pollution. Nevertheless, the average concentrations over all five sectors of eight of the species listed in Table 2 (CO_2, CO, SO_2, O_3, black particulate carbon, organic particulate carbon, total particle mass, and potassium particles) are greater than those that are typical of remote or rural locations.

[97] The average concentrations over all five sectors of CO_2 and CO (386 ± 8 ppmv and 261 ± 81 ppbv, respectively) exceed their corresponding typical background concentrations in remote or rural regions (~367 ppmv and ~50–150 ppbv, respectively). Since these long-lived trace gases are emitted during combustion, they indicate the impacts of biomass burning on air quality in southern Africa. The average SO_2 concentration over all five sectors (2.5 ± 1.6 ppbv) is comparable to the concentration of SO_2 that is typical of polluted urban air (~1.5 ppbv). This is attributable to emissions from mining, electric power generation, and biomass burning. The average O_3 concentration over all five sectors (64 ± 13 ppbv) exceeds that which is typical of remote locations (~20–40 ppbv). Since O_3 is an oxidant and a precursor to the OH radical, the elevated O_3 concentrations over southern Africa during the biomass burning season will tend to enhance the oxidative capacity of the troposphere in the region.

[98] The average concentrations of black carbon and organic carbon in all five sectors were 2.3 ± 1.9 $\mu g\ m^{-3}$ and 6.2 ± 5.2 $\mu g\ m^{-3}$, respectively; the latter value was derived from subtracting black carbon from total carbon in Table 2. These average concentrations fall within the range of concentrations of black carbon and organic carbon that are typical of polluted urban air (~1.5–20 $\mu g\ m^{-3}$ and 6–32 $\mu g\ m^{-3}$, respectively). The average ratio of black carbon to total carbonaceous particles over all five sectors (~0.27) is in the range typical of urban areas (~0.2–0.6). The average concentration of total particle mass over all five sectors (26.0 ± 4.7 $\mu g\ m^{-3}$) exceeds the ~15 $\mu g\ m^{-3}$ typical of rural locations; indeed, it approaches the concentrations for total particle mass typical of urban air (~32 $\mu g\ m^{-3}$). The high particle mass in the troposphere over southern Africa in the dry season is due primarily to smoke from biomass burning. The average over all five sectors of particulate potassium (0.40 ± 0.12 $\mu g\ m^{-3}$), the sources of which include biomass burning, is comparable to concentrations found in polluted continental air (~0.4–0.9 $\mu g\ m^{-3}$).

10. Summary and Conclusions

[99] In this paper we have presented measurements of the vertical distributions of temperature, relative humidity, SO_2, O_3, CN, and CO (Figures 6–10), and the horizontal distributions of twenty gaseous and particulate species (Table 2), over five sectors of southern Africa (Figure 2a) from August 14 to September 16 of 2000 during the dry biomass burning season. The Zambia and Botswana sectors had the highest concentrations of CO_2, CO, CH_4, ethane, propane, O_3, black particulate carbon, and total particulate carbon (Table 2). We attribute this primarily to the transport of smoke from biomass burning in Angola, Zimbabwe, South Africa, and Mozambique (Figures 3 and 11), as well as to local biomass burning.

[100] The South Africa sector had the highest concentrations of SO_2, sulfate, and CN (Table 2). The SO_2 concentrations were particularly high at the surface (Figure 6b), which we attribute to electric power generating plants, mining operations and biomass burning (Figure 3) within this sector.

[101] Air quality in the Mozambique sector was similar to the neighboring South Africa sector, with comparable concentrations of CO_2, CO, CH_4, O_3, organic particles, and inorganic particles (Table 2). Since there are few industrial sources of pollution in Mozambique, air quality was likely dominated by biomass burning within the sector (Figure 3) and the transport of pollutants from South Africa (Figure 11).

[102] The vertical distribution of pollutants over the arid Namibia sector can show a split structure, with a clean layer below ~2.5 km, and a polluted layer above ~2.5 km. Coastal stratus clouds are often located at about 1 km. In the polluted layer the mixing ratios of SO_2, O_3, and CO reached ~1.5 ppbv, ~80 ppbv, and ~275–375 ppbv, respectively (Figure 10). Back trajectories (Figure 11) and pollutant lifetimes indicate that transport of biomass smoke into the Namibia sector from intense savanna burning in southern Angola was responsible for the pollution aloft.

[103] When pollutant concentrations were averaged over all five sectors of this study, the concentrations of eight

species (CO_2, CO, SO_2, O_3, black carbon, organic particulate carbon, total particle mass, and potassium) were elevated above the concentrations typical of remote or rural continental locations (Table 2). For several of these species, the average concentrations over all five sectors approached values typical of polluted, urban air. Since most of the measurements in this study took place in locations well removed from industrial sources of pollution, the high average concentrations of pollutants in the lower troposphere reflect the impact of biomass burning (savanna fires and domestic) on the air quality of the region.

[104] Even locations with few biomass fires and industrial emissions, such as Namibia, can attain pollution levels comparable to those found in polluted urban air or in plumes from fires (Figure 10). In future work, the measurements reported here will be used to evaluate a regional atmospheric chemistry model.

[105] **Acknowledgments.** We thank all members of the UW-CARG and the pilots of the UW Convair-580 for their valuable help in obtaining measurements, and Dan Jaffe for help in calibrating the gas instruments. This study was carried out as part of the SAFARI 2000 Southern African Regional Science Initiative. Research support from grants NAG5-9022 and NAG5-7675 from NASA's Radiation Science Program, and grants ATM-9901624 and ATM-9900494 from NSF's Division of Atmospheric Sciences, is gratefully acknowledged.

References

Andreae, M. O., Soot carbon and excess fine potassium: Long-range transport of combustion-derived aerosols, *Science*, *220*, 1148–1151, 1983.

Andreae, M. O., and P. Merlet, Emission of trace gases and aerosols from biomass burning, *Global Biogeochem. Cycles*, *15*, 955–966, 2001.

Andreae, M. O., B. E. Anderson, D. R. Blake, J. D. Bradshaw, J. E. Collins, G. L. Gregory, G. W. Sachse, and M. C. Shipham, Influence of plumes from biomass burning on atmospheric chemistry over the equatorial and tropical South Atlantic during CITE 3, *J. Geophys. Res.*, *99*, 12,793–12,808, 1994.

Annegarn, H., R. Swap, S. Piketh, P. V. Hobbs, A. Queface, T. Freiman, D. Diner, and J. Kanyanga, "The river of smoke": Characteristics of the southern African springtime biomass burning haze, *J. Geophys. Res.*, in press, 2003.

Arino, O., and J.-M. Rosaz, 1997 and 1998 World ATSR Fire Atlas using ERS-2 ATSR-2 data, in *Proceedings of Joint Fire Science Conference*, pp. 177–182, Univ. of Idaho, Boise, 1999.

Bertschi, I., R. J. Yokelson, D. E. Ward, T. J. Christian, and W.-M. Hao, Trace gas emissions from the production and use of domestic biofuels in Zambia measured by open-path Fourier transform infrared (FTIR) spectroscopy, *J. Geophys. Res.*, *108*(D13), 8469, doi:10.1029/2002JD002158, 2003a.

Bertschi, I., R. J. Yokelson, D. E. Ward, R. E. Babbitt, R. A. Susott, J. G. Goode, and W. M. Hao, Trace gas and particle emissions from fires in large diameter and belowground biomass fuels, *J. Geophys. Res.*, *108*(D13), 8472, doi:10.1029/2002JD002100, 2003b.

Blake, N. J., D. R. Blake, B. C. Sieve, T. Y. Chen, F. S. Rowland, J. E. Collins Jr., G. W. Sachse, and B. E. Anderson, Biomass burning emissions and vertical distribution of atmospheric methyl halides and other reduced carbon gases in the South Atlantic region, *J. Geophys. Res.*, *101*, 24,151–24,164, 1996.

Bodhaine, B. A., Aerosol adsorption measurements at Barrow, Mauna Loa, and the south pole, *J. Geophys. Res.*, *100*, 8967–8975, 1995.

Cachier, H., C. Liousse, P. Buatmenard, and A. Gaudichet, Particulate content of savanna fire emissions, *J. Atmos. Chem.*, *22*, 123–148, 1995.

Chatfield, R. B., J. A. Vastano, L. Li, G. W. Sachse, and V. S. Connors, The Great African plume from biomass burning: Generalizations from a three-dimensional study of TRACE A carbon monoxide, *J. Geophys. Res.*, *103*, 28,059–28,077, 1998.

Colman, J. J., A. L. Swanson, S. Meinardi, B. C. Sive, D. R. Blake, and F. S. Rowland, Description of the analysis of a wide range of volatile organic compounds in whole air samples collected during PEM-Tropics A and B, *Anal. Chem.*, *73*, 3723–3731, 2001.

Cosijn, C., and P. D. Tyson, Stable discontinuities in the atmosphere over South Africa, *S. Afr. J. Sci.*, *92*, 381–385, 1996.

Crutzen, P. J., and M. O. Andreae, Biomass burning in the tropics: Impact on atmospheric chemistry and biogeochemical cycles, *Science*, *250*, 1669–1678, 1990.

de Laat, A. T. J., On the origin of tropospheric O_3 over the Indian Ocean during the winter monsoon: African biomass burning vs. stratosphere-troposphere exchange, *Atmos. Chem. Phys.*, *2*, 325–341, 2002.

Diab, R. D., et al., Vertical ozone distribution over southern Africa and adjacent oceans during SAFARI-92, *J. Geophys. Res.*, *101*, 23,823–23,833, 1996.

Eatough, D. J., N. L. Eatough, Y. Pang, S. Sizemore, T. W. Kirchstetter, T. Novakov, and P. V. Hobbs, Semivolatile particulate organic materials in southern Africa during SAFARI 2000, *J. Geophys. Res.*, *108*(D13), 8479, doi:10.1029/2002JD002296, 2003.

Energy Information Administration (EIA), Southern Africa and the Southern African Development Community, Washington, D. C., 2002. (Available at www.eia.doe.gov/emeu/cabs/sadc.html)

Finlayson-Pitts, B. J., and J. N. Pitts Jr., *Chemistry of the Upper and Lower Atmosphere*, Academic, San Diego, Calif., 2000.

Fishman, J., K. Fakhruzzaman, B. Cros, and D. Nganga, Identification of widespread pollution in the southern hemisphere deduced from satellite analyses, *Science*, *252*, 1693–1696, 1991.

Fishman, J., J. M. Hoell, R. D. Bendura, R. J. McNeil, and V. W. J. H. Kirchhoff, NASA GTE TRACE A experiment (September–October 1992): Overview, *J. Geophys. Res.*, *101*, 23,869–23,879, 1996.

Freiman, M. T., M. R. Jury, and S. Medcalf, The state of the atmosphere over South Africa during the Southern African Regional Science Initiative (SAFARI 2000), *S. Afr. J. Sci.*, *98*, 91–96, 2002.

Gao, S., D. A. Hegg, P. V. Hobbs, T. W. Kirchstetter, B. Magi, and M. Sadelik, Water-soluble organic components in aerosols associated with savanna fires in southern Africa: Identification, evolution, and distribution, *J. Geophys. Res.*, *108*(D13), 8491, doi:10.1029/2002JD002324, 2003.

Goode, J. G., R. J. Yokelson, D. E. Ward, R. A. Susott, R. E. Babbitt, M. A. Davies, and W. M. Hao, Measurements of excess O_3, CO_2, CO, CH_4, C_2H_4, C_2H_2, HCN, NO, NH_3, HCOOH, CH_3COOH, HCHO, and CH_3OH in 1997 Alaskan biomass burning plumes by airborne Fourier transform infrared spectroscopy (AFTIR), *J. Geophys. Res.*, *105*, 22,147–22,166, 2000.

Gundel, L. A., R. L. Dod, H. Rosen, and T. Novakov, The relationship between optical attenuation and black carbon concentrations for ambient and source particles, *Sci. Total Environ.*, *36*, 197–202, 1984.

Hao, W. M., and M. H. Liu, Spatial and temporal distribution of tropical biomass burning, *Global Biogeochem. Cycles*, *8*, 495–503, 1994.

Hobbs, P. V., *Introduction to Atmospheric Chemistry*, Cambridge Univ. Press, New York, 2000.

Hobbs, P. V., Atmosphere science: Clean air slots amid atmospheric pollution, *Nature*, *415*, 861, 2002.

Hobbs, P. V., Clean air slots amid dense atmospheric pollution in southern Africa, *J. Geophys. Res.*, *108*(D13), 8490, doi:10.1029/2002JD002156, 2003.

Hobbs, P. V., J. S. Reid, J. A. Herring, J. D. Nance, R. E. Weiss, J. L. Ross, D. A. Hegg, R. D. Ottmar, and C. Liousse, Particle and trace-gas measurements in the smoke from prescribed burns of forest products in the Pacific northwest, in *Biomass Burning and Global Change*, vol. 2, edited by J. S. Levine, pp. 697–715, MIT Press, Cambridge, Mass., 1996.

Hobbs, P. V., P. Sinha, R. J. Yokelson, T. J. Christian, D. R. Blake, S. Gao, T. W. Kirchstetter, T. Novakov, and P. Pilewskie, Evolution of gases and particles from a savanna fire in South Africa, *J. Geophys. Res.*, *108*(D13), 8485, doi:10.1029/2002JD002352, 2003.

Huntley, B. J., Southern African savannas, in *Ecology of Tropical Savannas*, edited by B. J. Huntley and B. H. Walker, pp.101–119, Springer-Verlag, New York, 1982.

Intergovernmental Panel on Climate Change (IPCC), *Climate Change 2001: The Scientific Basis*, Cambridge Univ. Press, New York, 2001.

Jacob, D. J., et al., The origin of ozone and NO_x in the tropical troposphere: A photochemical analysis of aircraft observations over the South Atlantic Basin, *J. Geophys. Res.*, *101*, 24,235–24,250, 1996.

Jury, M. R., The dry season climate of tropical southern Africa and implications for pyrogenic emissions, *S. Afr. J. Sci.*, *96*, 387–390, 2000.

Justice, C. O., J. D. Kendall, P. R. Dowty, and R. J. Scholes, Satellite remote sensing of fires during the SAFARI campaign using NOAA advanced very high resolution radiometer data, *J. Geophys. Res.*, *101*, 23,851–23,863, 1996.

Kirchstetter, T. W., T. Novakov, P. V. Hobbs, and B. Magi, Airborne measurements of carbonaceous aerosols in southern Africa during the biomass burning season, *J. Geophys. Res.*, *108*(D13), 8476, doi:10.1029/2002JD002171, 2003.

Li, J., M. Pósfai, P. V. Hobbs, and P. R. Buseck, Individual aerosol particles from biomass burning in southern Africa: 2. Compositions and aging of inorganic particles, *J. Geophys. Res.*, *108*(D13), 8484, doi:10.1029/2002JD002310, 2003.

Liousse, C., H. Cachier, and S. G. Jennings, Optical and thermal measurements of black carbon aerosol content in different environments—Variation

of the specific attenuation cross-section, sigma (σ), *Atmos. Environ.*, *27*, 1203–1211, 1993.

Liousse, C., C. Devaux, F. Dulac, and H. Cachier, Aging of savanna biomass aerosols: Consequences on their optical properties, *J. Atmos. Chem.*, *22*, 1–17, 1995.

Magi, B. I., and P. V. Hobbs, Effects of humidity on aerosols in southern Africa during the biomass burning season, *J. Geophys., Res.*, *108*(D13), 8495, doi:10.1029/2002JD002144, 2003.

Magi, B. I., P. V. Hobbs, B. Schmid, and J. Redemann, Vertical profiles of light, scattering, light absorption, and single scattering albedo during the dry, biomass burning season in southern Africa and comparisons of in situ and remote sensing measurements of aerosol optical depths, *J. Geophys. Res.*, *108*(D13), 8504, doi:10.1029/2002JD002361, 2003.

Mano, S., and M. O. Andreae, Methyl bromide from biomass burning, *Science*, *263*, 1255–1256, 1994.

Mauzerall, D. L., J. A. Logan, D. J. Jacob, B. E. Anderson, D. R. Blake, J. D. Bradshaw, B. Heikes, G. W. Sachse, H. Singh, and B. Talbot, Photochemistry in biomass burning plumes and implications for tropospheric ozone over the tropical South Atlantic, *J. Geophys. Res.*, *103*, 8401–8423, 1998.

McGregor, G. R., and S. Nieuwolt, *Tropical Climatology*, John Wiley, Hoboken, N. J., 1998.

Moosmuller, H., W. P. Arnott, C. F. Rogers, J. C. Chow, C. A. Frazier, L. E. Sherman, and D. L. Dietrich, Photoacoustic and filter measurements related to aerosol light absorption during the Northern Front Range Air Quality Study (Colorado 1996/1997), *J. Geophys. Res.*, *103*, 28,149–28,157, 1998.

Novakov, T., Microchemical characterization of aerosols, in *Nature, Aim and Methods of Microchemistry*, edited by H. Malissa, M. Grasserbaure, and R. Belcher, pp. 141–165, Springer-Verlag, New York, 1981.

Novakov, T., Soot in the atmosphere, in *Particulate Carbon: Atmospheric Life Cycle*, edited by G. T. Wolff and R. L. Klimish, pp. 19–41, Plenum, New York, 1982.

Petzold, A., C. Kopp, and R. Niessner, The dependence of the specific attenuation cross-section on black carbon mass fraction and particle size, *Atmos. Environ.*, *31*, 661–672, 1997.

Pilewskie, P., J. Pommier, R. Bergstrom, W. Gore, S. Howard, M. Robbette, B. Schmid, P. V. Hobbs, and S.-C. Tsay, Solar spectral radiative forcing by aerosols during SAFARI 2000, *J. Geophys. Res.*, *108*(D13), 8486, doi:10.1029/2002JD002411, 2003.

Pósfai, M., R. Simonics, J. Li, P. V. Hobbs, and P. R. Buseck, Individual aerosol particles from biomass burning in southern Africa: 1. Compositions and size distributions of carbonaceous particles, *J. Geophys. Res.*, *108*(D13), 8483, doi:10.1029/2002JD002291, 2003.

Privette, J., D. Landis, J. Nickeson, and J. Morisette, *SAFARI 2000 CD-ROM Series*, vol. 1, NASA Goddard Space Flight Cent., Greenbelt, Md., July 2001.

Reid, J. S., P. V. Hobbs, R. J. Ferek, D. R. Blake, J. V. Martins, M. R. Dunlap, and C. Liousse, Physical, chemical, and optical properties of regional hazes dominated by smoke in Brazil, *J. Geophys. Res.*, *103*, 32,059–32,080, 1998.

Rosen, H., and T. Novakov, Optical-transmission through aerosol deposits on diffusely reflective filters—A method for measuring the absorbing component of aerosol-particles, *Appl. Opt.*, *22*, 1265–1267, 1983.

Sawa, Y., H. Matsueda, Y. Tsutsumi, J. B. Jensen, H. Y. Inoue, and Y. Makino, Tropospheric carbon monoxide and hydrogen measurements over Kalimantan in Indonesia and northern Australia during October 1997, *Geophys. Res. Lett.*, *26*, 1389–1392, 1999.

Schmid, B., et al., Coordinated airborne, spaceborne, and ground-based measurements of massive, thick aerosol layers during the dry season in southern Africa, *J. Geophys. Res.*, *108*(D13), 8496, doi:10.1029/2002JD002297, 2003.

Seinfeld, J. H., and S. N. Pandis, *Atmospheric Chemistry and Physics*, John Wiley, Hoboken, N. J., 1998.

Silva, J. M. N., J. M. C. Pereira, A. I. Cabral, A. C. L. Sá, M. J. P. Vasconcelos, B. Mota, and J.-M. Grégoire, An estimate of the area burned in southern Africa during the 000 dry season using SPOT-VEGETATION satellite data, *J. Geophys. Res.*, *108*(D13), 8498, doi:10.129/2002JD002320, 2003.

Sinha, P., P. V. Hobbs, R. J. Yokelson, I. T. Bertschi, D. R. Blake, I. J. Simpson, S. Gao, T. W. Kirchstetter, and T. Novakov, Emissions of trace gases and particles from biomass burning in southern Africa, *J. Geophys. Res.*, *108*(D13), 8487, doi:10.1029/2002JD002325, 2003a.

Sinha, P., P. V. Hobbs, R. J. Yokelson, T. J. Christian, T. W. Kirchstetter, and R. Bruintjes, Emissions of trace gases and particles from two ships in the southern Atlantic Ocean, *Atmos. Environ.*, *37*, 2139–2148, 2003b.

Thompson, A. M., K. E. Pickering, D. P. McNamara, M. R. Schoeberl, R. D. Hudson, J. H. Kim, E. V. Browell, V. W. J. H. Kirchhoff, and D. Nganga, Where did tropospheric ozone over southern Africa and the tropical Atlantic come from in October 1992? Insights from TOMS, GTE TRACE A, and SAFARI 1992, *J. Geophys. Res.*, *101*, 24,251–24,278, 1996.

Thompson, A. M., J. C. Witte, M. T. Freiman, N. A. Phahlane, and G. J. R. Coetzee, Lusaka, Zambia, during SAFARI-2000: Convergence of local and imported ozone pollution, *Geophys. Res. Lett.*, *29*(20), 1976, doi:10.1029/2002GL015399, 2002.

U.S. Environmental Protection Agency (U.S. EPA), Compilation of air pollutant emission factors, in *Final Section—Supplement E: External Combustion Sources*, 5th ed., vol. 1, chap. 1, *Rep. AP-42*, Washington, D. C., 1998.

Warneck, P., *Chemistry of the Natural Atmosphere*, Academic, San Diego, Calif., 2000.

White, F., UNESCO/AETFAT/UNSO vegetation map of Africa, U. N. Educ., Sci., and Cult. Org., Paris, 1981.

White, F., Vegetation of Africa, U. N. Educ., Sci., and Cult. Org., Paris, 1983.

Wingenter, O. W., C. J.-L. Wang, D. R. Blake, and F. S. Rowland, Seasonal variation of tropospheric methyl bromide concentrations: Constraints on anthropogenic input, *Geophys. Res. Lett.*, *25*, 2797–2800, 1998.

Yasa, Z., N. M. Amer, H. Rosen, A. D. A. Hansen, and T. Novakov, Photoacoustic investigation of urban aerosol particles, *Appl. Opt.*, *18*, 2528–2530, 1979.

Yevich, R., and J. A. Logan, An assessment of biofuel use and burning of agricultural waste in the developing world, *Global Biogeochem.*, *17*, doi:10.1029/2002GB001952, in press, 2003.

Yokelson, R. J., D. W. T. Griffith, and D. W. Ward, Open-path Fourier transform infrared studies of large-scale laboratory biomass fires, *J. Geophys. Res.*, *101*, 21,067–21,080, 1996.

Yokelson, R. J., I. T. Bertschi, T. J. Christian, P. V. Hobbs, D. E. Ward, and W. M. Hao, Trace gas measurements in nascent, aged, and cloud-processed smoke from African savanna fires by airborne Fourier transform infrared (AFTIR) spectroscopy, *J. Geophys. Res.*, *108*(D13), 8478, doi:10.1029/2002JD002322, 2003.

D. R. Blake, Department of Chemistry, University of California, Irvine, CA 92717, USA.

S. Gao, Department of Environmental Science and Engineering, California Institute of Technology, Pasadena, CA 91125, USA.

P. V. Hobbs and P. Sinha, Department of Atmospheric Sciences, University of Washington, Box 351640, Seattle, WA 98195-1640, USA. (phobbs@atmos.washington.edu)

T. W. Kirchstetter, Lawrence Berkeley National Laboratory, Berkeley, CA 94720, USA.

R. J. Yokelson, Department of Chemistry, University of Montana, Missoula, MT 59801, USA.